

Chapter 7

Handheld Probe-Based Dual Mode Ultrasound/Photoacoustics for Biomedical Imaging

Mithun Kuniyil Ajith Singh, Wiendelt Steenbergen
and Srirang Manohar

Abstract Photoacoustic (PA) imaging is a promising biomedical imaging modality that has emerged over the last decade. In this method, imaging is performed using pulsed far-red or near-infrared light. This light while scattering through soft tissue is absorbed at specific locations by certain molecules such as hemoglobin in blood. The absorbed energy is converted into heat; the subsequent thermoelastic expansion causes ultrasound (US) to be produced from the absorbing region. The US is measured at the surface of tissue using US detectors and the acquired signals are used to reconstruct the location and spatial details of the absorber. PA imaging thus combines the advantages of optical and US imaging, providing excellent optical spectroscopic contrast with ultrasonic resolution. While US imaging utilizes acoustic impedance mismatches in tissue for its signals to provide structural details, PA imaging extracts functional information based on optical absorption by chromophores, predominantly blood, and often exogenous contrast agents. Since PA imaging involves US detection, it can be seamlessly implemented in a commercially available US scanner to perform dual mode PA/US imaging, which is a promising translational medical diagnostic technique. These dual mode systems providing complementary contrast hold potential for myriad of clinical applications. Handheld dual mode US/PA probes use reflection mode imaging geometry, where light irradiation is done from the same side where PA signals are detected. These epi-style handheld probe-based imaging setup delivers flexibility in imaging different body parts using the same probe. This review details the fundamentals of PA/US imaging and also depicts the importance of handheld probe-based dual mode PA/US systems. Particular attention is paid to the engineering aspects of systems developed by different groups and range of clinical applications demonstrated by them.

M. Kuniyil Ajith Singh (✉) · W. Steenbergen · S. Manohar (✉)
University of Twente, Biomedical Photonic Imaging Group, MIRA Institute,
P.O. Box 217, 7500 AE Enschede, The Netherlands
e-mail: m.kuniyilajithsingh@utwente.nl

S. Manohar
e-mail: s.manohar@utwente.nl

1 Introduction

Medical imaging provides crucial information that assists decision making for choosing the course of action and suitable therapy. Imaging can contribute to detection of the occult disease, and accurate diagnosis, which can enable timely intervention, precluding complex medication and surgery at late stages of disease. Imaging technologies strive to achieve this at an affordable cost with minimal patient burden. Examples of modalities that are present in most specialist hospitals are: ultrasound (US) imaging, x-ray imaging, Magnetic Resonance Imaging (MRI), x-ray Computed Tomography, Positron Emission tomography (PET) etc. The techniques can be fundamentally different in the physics of the interaction of the energy probe with tissue, in contrast mechanisms, and in the applications. The technologies are different in terms of initial expense, and infrastructure and maintenance requirements, and in their performance parameters.

Of the methods used, US imaging is largely ubiquitous in clinics owing to its compactness, relative affordability and real-time performance especially for point of care applications. A recent innovation is development of a hybrid modality bringing together US imaging with photoacoustic (optoacoustic) imaging. The latter is a new method that uses pulsed laser light to excite US from within tissue from absorbing structures such as blood vessels. While US imaging has a long history, photoacoustic (PA) imaging is at the stage of early proof-of-principle clinical studies in research hospitals, but is expected to have an impact in health care in the near future. Handheld probe-based dual mode systems combining US and PA imaging holds promise as a potential technique for translational biomedical imaging.

In this chapter, we review various handheld probe-based systems capable of performing both US and PA imaging, and their myriad applications. The first section provides an overview of the existing optical and US imaging techniques, followed by a detailed description of PA imaging. Furthermore, this section briefly discusses the importance of hand held and portable systems in clinical settings. The second section presents the engineering aspects of handheld dual mode US/PA systems currently being investigated and tested, and different applications that are explored and foreseen.

1.1 Optical Imaging

Optical tissue imaging, makes use of spectroscopic features of light-tissue interactions such as scattering, absorption and polarization [1]. Since many physiological molecules in tissue possess characteristic wavelength-dependent absorptions (Fig. 1), this interaction is most powerful for interrogating tissues at functional and molecular levels [2]. The molecules of interest are typically hemoglobin (Hb), oxyhemoglobin (HbO₂), melanin, lipids and water, each with a signature optical absorption spectrum [3].

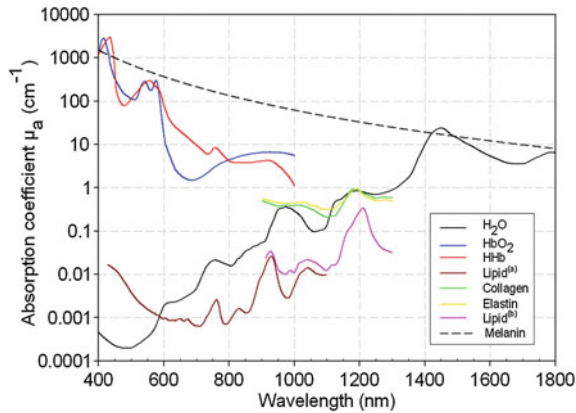


Fig. 1 Absorption coefficient spectra of endogenous tissue chromophores. Oxyhemoglobin (*red line*), deoxyhemoglobin (*blue line*), water (80 % by volume in tissue, *black line*), lipid **a** (20 % by volume in tissue, *brown line*), lipid **b** (*pink line*), melanin (μ_a corresponds to that in skin, *black dashed line*), Collagen (*green line*) and elastin (*yellow line*) (Reprinted from Ref. [7]. With permission from the author and Royal Society Publishing)

The relative presence of these chromophores can often be linked to different disease conditions. For example, increased hemoglobin can be a sign of angiogenesis, growth of new blood vessels, which is often associated with a variety of oncological [4] and inflammatory diseases [5]. Further, angiogenesis is also a natural tissue response for promoting wound and burn healing [1], and can be a marker for monitoring this process. The ratio of HbO to total hemoglobin ($H_t = Hb + HbO$) or oxygen saturation, in the microcirculation, is expected to be lower in cancer due to increased oxygen consumption associated with high metabolism, which could be a marker of the disease [6]. Melanin serves as the marker for melanoma detection and evaluation using optical imaging techniques.

The rich spectroscopic contrast of these molecules and their relation to a spectrum of diseases make optical imaging versatile. However, purely light-based imaging techniques suffer from poor resolution at depths larger than a few mm, due to high scattering in tissue [8].

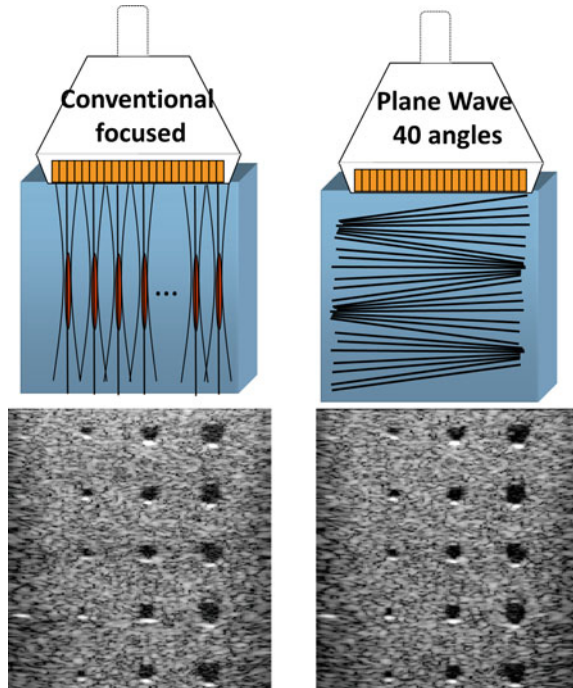
1.2 Ultrasound Imaging

US imaging is able to visualize anatomy from echoes of US pulses insonifying the tissue [9, 10]. The method has a long history of development with the first US detector arrays in use since the 1970s [11]. One of the latest developments in the field is acquisition of ultrafast frame rates for real-time visualization of flow and transient elastography. This is possible with the use of plane waves in which a large area is insonified with single emission from the entire aperture, with the

backscattered echoes detected by all elements for building up the image [12]. Multiple images are acquired by steering the plane waves into the object at various angles, and these are compounded either incoherently to reduce speckle and improve contrast, or coherently to improve resolution. Such an approach can realize several hundreds of frames per sec (fps) with the image quality approaching standard multi-focus US imaging with lower frame rates.

Despite all these developments in technology, US imaging fundamentally suffers from poor soft-tissue contrast. While it has various applications for which it is suited, such as differentiating between solid masses and fluid filled cysts, the method is not sufficiently specific or sensitive [13] for discrimination between malignancies and benign abnormalities. Speckle noise in US images degrades contrast which limits its applicability in imaging heterogeneous environments [14]. However the defining advantages of US imaging are the capability to perform real-time imaging, and the fact that low scattering in tissue allows the phase to be preserved, providing the capability to focus US and generally attain excellent resolution even at larger depths [15]. This is in contrast to optical imaging methods where the scattering is 2–3 orders stronger [16]. Figure 2 shows speed and contrast differences of conventional focused US and plane wave compounding making use of transmission at 40 angles.

Fig. 2 Conventional focused and ultrafast ultrasound imaging sequence for a typical medical imaging setup (4 cm deep region of interest): *left* conventional focused imaging (128 focused beams and 4 focal depths leading to ~ 25 fps), *right* plane-wave compounding with 40 angles (~ 350 fps). (Adapted from Ref. [12]. With permission from the authors and IEEE)



1.3 Photoacoustic Imaging

In photoacoustic imaging, the advantages of the high contrast of optical imaging, and the high resolution of US imaging are brought together. Here pulsed light absorbed by the target emits US by a thermoelastic mechanism. This US is detected and used to build up an image [17]. The effect has its roots in early work by Alexander Graham Bell in 1880 who observed sound generation from certain dark materials exposed to modulated sunlight [18]. The first work on using the pulsed PA effect potentially for medical imaging application was reported in the mid-1990s [19–21]. Since then there has been steady growth in the field with several embodiments of the technology, and various demonstrations of potential applications.

1.3.1 Photoacoustic Signal Generation Process

Figure 3 illustrates the photoacoustic effect in biological tissue. Short pulsed laser light is shone on the tissue, and depending on the wavelength the photons will undergo scattering and absorption [7]. This absorbed laser energy initiates a temperature rise, which then leads to an expansion of the absorbing structure. Under stress and thermal confinement conditions, this causes an initial pressure increase and the subsequent emission of US waves, which propagate to the surface where they are detected. Stress confinement is met when the generated photoacoustic waves are not travelling longer than the size of light absorber, during the course of the light excitation pulse. This is fulfilled if the sound velocity multiplied by the pulse duration of the laser is small compared to the size of the light absorbing structure. Thermal confinement is met when the heat generated by the absorber is not diffusing more than the size of the absorber during the course of the light excitation pulse. As heat diffusion is usually slower than the propagation of sound, the thermal confinement is fulfilled if stress confinement is fulfilled. Theoretically,

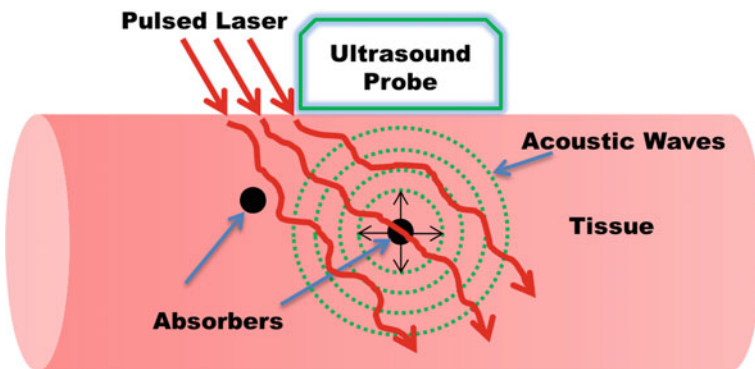


Fig. 3 Schematic illustration of the photoacoustic effect in biological tissue

only 1 milliKelvin temperature can generate about 800 Pa pressure rise which then can be detected by a typical ultrasonic transducer [8].

PA signal generation can be regarded as an optical absorption-induced pressure distribution p_0 from which US waves propagate to the surface of tissue to be transduced into time resolved electric signals using US detectors. Images are formed by acquiring signals from multiple spatial points. Since US undergoes low scattering and absorption, a PA image can be considered in the first approximation as an image space representation of p_0 [7]. Under conditions of stress and heat confinement, the initial pressure distribution p_0 at a point r is proportional to $H(r)$, the absorbed optical energy density [22].

$$p_0(r) = \Gamma H(r) \quad (1)$$

Here Γ is the Grüneisen coefficient, a dimensionless thermodynamic constant which describes the conversion efficiency of heat energy to pressure. It is given by $\Gamma = \beta c^2 / C_p$, where β is the volume thermal expansion coefficient, c the speed of sound and C_p the specific heat capacity at constant pressure. The absorbed optical energy $H(r)$ is the product of the local absorption coefficient $\mu_a(r)$ and the optical fluence $\Phi(r, \mu_a, \mu_s, g)$ where μ_a and μ_s are the absorption and scattering coefficients over the illuminated tissue volume with g the anisotropy factor. So p_0 can be written as follows

$$p_0(r) = \Gamma \mu_a(r) \Phi(r, \mu_a, \mu_s, g), \quad (2)$$

Equation 2 shows that $p_0(r)$ while depending explicitly on local μ_a also depends via the fluence globally on μ_a and μ_s in tissue through which photons have traversed to r . Thus image contrast is not directly proportional to μ_a , but to the product of μ_a and Φ with the fluence itself depending on μ_a making p_0 a nonlinear function of μ_a [7]. Further, $p_0(r)$ also depends on mechanical and thermodynamic parameters via Γ which may also change depending on position [23]. Nevertheless for a qualitative treatment, the PA image can be thought to represent the spatial distribution of absorbed optical energy $H(r)$ in tissue.

1.3.2 Photoacoustic Image Reconstruction

Since the method relies on optical contrast and US propagation-detection, reconstruction tools and analyses borrow from the two areas of diffuse optics and US. Basic PA reconstruction serves to retrieve the spatial distribution of the acoustic sources or locations of optical energy deposition. This is termed the acoustic inversion problem and uses various algorithms from the US and sonar world. From the distribution of acoustic sources one would like to estimate a representation of the optical absorption coefficient distribution, but as discussed earlier, this is a non-linear problem. Reconstruction of optical absorption coefficient is termed quantitative PA imaging.

In this review of combined PA-US systems, we focus on basic PA image reconstruction schemes which resemble the methods for reconstructing medical US data. The main differences between US and PA image reconstructions are: (1) the time of flight is half in PA imaging, since the acoustic waves are generated within tissue and not by backscattering of ultrasound as in US imaging, (2) the frequency content of detected signals in PA is different based on the sizes of the absorbers, while that in US imaging is generally the same as the injected frequencies.

A review of the mathematics behind reconstruction approaches in PA imaging is given in Kuchment et al. [24]. The reconstruction algorithms are selected based on the geometry of receiving elements, computing speed available etc. As this chapter focuses on handheld probe-based systems, which mainly make use of linear array transducers, discussion about reconstruction algorithms will be limited to those which are practically being applied for these geometries.

The filtered back-projection algorithm is commonly applied for PA data due to its simplicity and speed [7]. Figure 4 shows the basic idea behind the algorithm for a PA linear/planar detection geometry. In back-projection PA tomography image reconstruction for a planar detection geometry, PA waveforms are recorded by each detector element of the US probe at specific location, spatially resolved using the sound speed c and back-projected over spherical surface of radius $R = ct$ into the imaging volume [7]. The recorded pressure waveforms are time integrated computationally in this case.

The method is analogous to delay and sum beam-forming employed in phased array US imaging [23]. A delay and sum beam-forming algorithm used for image reconstruction in a US imaging system can be used for PA image reconstruction just by reducing the time of flight to half. This easy switching between reconstruction algorithms is important for dual modality PA-US imaging systems. Although both

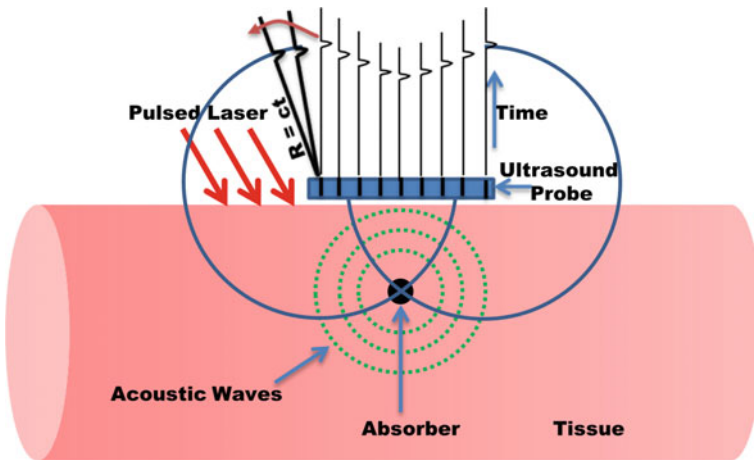


Fig. 4 Backprojection PAT image reconstruction for a planar detection geometry

methods give simple and clear description about PA image formation, it is not the finest in terms of precision and computational overhead. The time reversal method is also gaining in popularity due to the availability of a freely available third party MATLAB toolbox, which performs image reconstruction using k -space methods [25].

An algorithm based on harmonic decomposition of the pressure waves arising from the object has been used in linear/planar detection geometries. Since the computation overhead is important, this approach is attractive since most of the processing is done via the fast Fourier transform and a k -space interpolation [7]. The use of the frequency-domain approach permits reconstruction and presentation of the resultant image in real-time, a key criterion for a PA system developed around a US scanner. Several groups have reported on fast algorithms based on frequency domain processing [26, 27]. Systems have been presented that can do real time reconstruction of PA images [28–30], and some others based on recent developments in GPU technology which can do real-time PA and US imaging [14].

1.4 Handheld Ultrasound/Photoacoustic Imaging Systems—Motivation

Imaging tests on patients are usually done using various modalities in sequence to extract the necessary information from the suspect region or organ to decide the course of action. Multimodality imaging combining two complementary techniques, is of interest to reduce the need for multiple or layered imaging. PA imaging can be combined with US imaging with relative ease since the acoustic hardware required for both techniques can be shared. A dual mode system combines the advantages of both modalities. A US image superimposed on a PA image can give anatomical and structural information overlaid with rich detail of functions. The versatility of such a system is further improved by the availability of US Doppler imaging and elasticity imaging [31].

In addition to the convenient visualization of complementary information, estimated parameters from US imaging such as speed of sound (SOS) and acoustic attenuation (AA) can be utilized into PA imaging in an iterative framework to improve the accuracy of the reconstruction. This can play an important role in enabling quantitative PA imaging [32, 33].

Further, PA is a new technology seeking to make inroads into the clinic, while US is an accepted modality in healthcare. From the point of view of PA, the incorporation of PA into a dual modality system with US can potentially have relatively easier clinical acceptance [28, 33]. The impact and importance of a system that can perform co-registered US and PA imaging using a handheld probe, which is clinically acceptable, is high considering the vital point of care applications in diagnostic imaging and treatment monitoring.

2 Handheld Probe-Based US/PA Systems and Applications

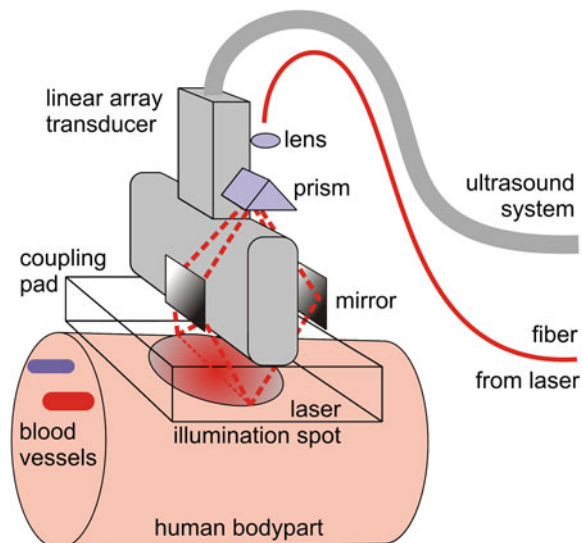
2.1 The University of Bern System

The first report of a combined PA-US system using a handheld probe was from the Bern group [27] in collaboration with the Fraunhofer Institute (St. Ingbert, Germany). A custom made high-speed US system was developed that could simultaneously perform PA imaging. The 128-element linear array used had a center frequency of 7.5 MHz (LA/7.5/128/ULS, Vermon S.A, France). Light illumination was provided from a Q-switched Alexandrite laser emitting short near-infrared laser pulses (60 ns) at a wavelength of 760 nm.

The laser light was coupled to a 400 μm optical fiber, and using a prism and two mirrors (Fig. 5) was split into two beams and delivered to the object from either side of the probe, giving a homogeneously illuminated spot of diameter 25 mm. The radiant exposure was under $5 \text{ mJ}/\text{cm}^2$, below the maximum permissible exposure (MPE) of $20 \text{ mJ}/\text{cm}^2$.

The system was connected to a dual processor computer, which allowed for real time reconstruction at 7.5 fps using a modified Fourier reconstruction algorithm [34]. For US-echography, a conventional digital beam-former with time gain compensation (TGC) amplifier and dynamic aperture were used on 16 channels. Proper adjustments were done in the reconstruction software between the two modalities. Since parallel acquisition was used, only one pulse was enough for recording a complete frame, and reconstruction was done in less than 100 ms. The system had the capability of displaying a PA image alongside the classical US image. With this system, the lateral resolution achievable was defined by the NA of

Fig. 5 Dual mode photoacoustic and ultrasound real-time imaging setup. (Reprinted from Ref. [27]. With permission from the authors and IEEE)



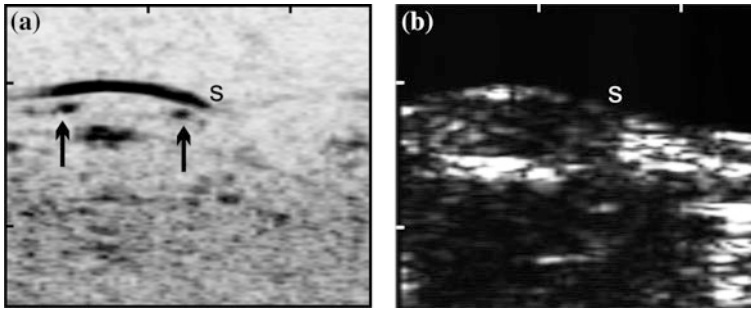


Fig. 6 **a** Photoacoustic image and **b** ultrasound image of a human index finger (palm toward transducer). (Reprinted from Ref. [27]. With permission from the authors and IEEE)

the ‘lens’ formed by all active detector elements and the average US wavelength (associated with the centre frequency of the array), and the axial resolution of 0.3 mm was defined by the bandwidth of the transducer (5.5 MHz). The transducer was sensitive to blood vessels in the range of 100–300 μm corresponding to signal frequencies of 4.5–10 MHz within the bandwidth. The system was not sensitive to smaller vessels compared to the larger ones, and the larger vessels also showed distortions such as edge oscillations in the reconstructions.

The system demonstrated the importance of parallel data acquisition and fast image reconstruction. However the system made use of a custom-made data acquisition set up which would more likely be expensive when compared to systems derived from preexisting commercial US scanners.

Figure 6a shows the PA image and (b) the US image of a healthy human index finger measured using this system. The images cover a 2.6×2.0 cm area (ticks every cm) with the transducer at the top of the images. On the PA image (left) the skin is visible as an arc shaped black line (s). At 1 mm below the skin the *Vv. digitales palmares* are visible as two black dots on either side of the finger (arrows). They are accompanied by the corresponding *Aa. digitales palmares propriae*, which appear much fainter (tiny dots besides veins) because of the reduced absorption of oxyhemoglobin at 760 nm. Below the skin, at 3 mm depth, a blood perfused region possibly the periosteum is visible. The four vessels and the periosteum are not visible in the corresponding US image (right). The US image is predominated by the echo signal from the skin (s) and the large echo signal from the bone 5 mm below it. The skin surface position matches well on both images; it is, however, obvious that the two methods extract complementary information.

2.2 The Twente Systems

The Twente group in collaboration with ESAOTE Europe BV developed a dual modality imaging system, one of the first attempts in using a commercial US scanner (Picus, ESAOTE Europe BV, Maastricht, the Netherlands) for PA imaging

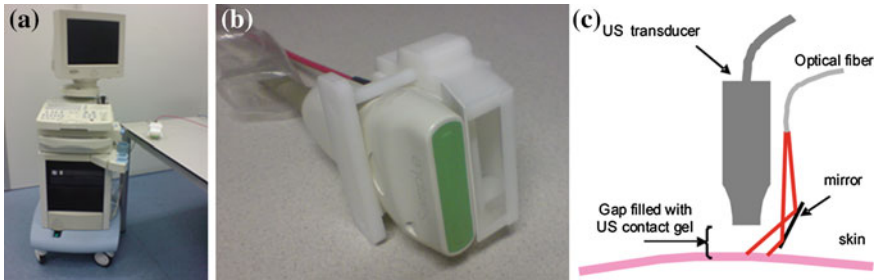


Fig. 7 **a** Ultrasound system (Picus, ESAOTE Europe BV, Maastricht the Netherlands). **b** Optical module connected to US probe. **c** Schematic overview of optical system connected to US probe. (Adapted from Ref. [30, 35]. With permission from the authors and SPIE)

[30, 35]. The system used a linear array (L10-5, 40 mm, 7.5 MHz central frequency, 128 elements, ESAOTE Europe BV) transducer. Light pulses (8 ns) from a 1 kHz Nd:YAG laser (1064 nm) were coupled to a 600 μm optical fiber which terminated in an optical module fitted to the US array (Fig. 7b). The custom-made module was composed of a beam expander, a cylindrical lens and a stationary mirror that illuminated an area of $5 \times 20 \text{ mm}^2$ (Fig. 7c).

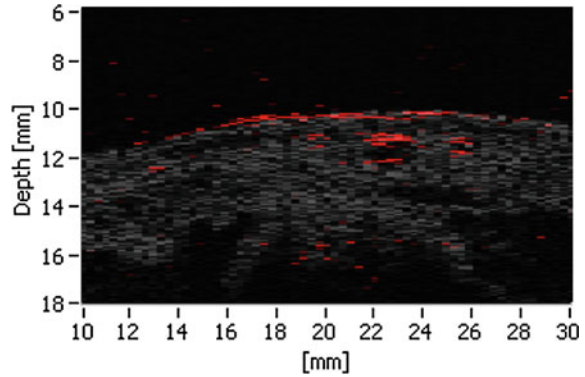
The changes made to incorporate PA imaging, were synchronization of the data-acquisition with the firing of the laser and an option to switch-off the emission of US. A sequential line-by-line scanning approach was employed, requiring 128 laser pulses for a frame. At a pulse repetition rate of 1 kHz, this resulted in a frame rate of 8 fps. All the required modifications mentioned and changes in reconstruction algorithm were achieved without affecting the system's performance for conventional US imaging.

Center frequency (7.5 MHz) and bandwidth (75 % -6 dB) of the US transducer limited the sensitivity of the system to visualize structures larger than 100 μm . This real-time US/PA system had the advantage that it made use of a commercial US scanner, which precluded the need for high-speed digitizers and computers for data acquisition and reconstruction of images.

Overlay images of measurements on the dorsal side of a volunteer's hand are shown in Fig. 8. PA signals from the skin and blood vessels are clearly visible and US here supports to identify boundaries and bone. The largest blood vessel (axial diameter 1.22 mm) visualized in the PA data ($x = 22 \text{ mm}$, depth = 12 mm) is visible in the US image as a hypoechoic region. Smaller vessels present in the PA image are not visible in US. The bone is visualized as a semicircular structure with low backscatter intensity in the US image ($x = 16\text{--}26 \text{ mm}$, depth = 15–18 mm). PA signal reflection artefacts are present in the image at a depth of around 16–18 mm. US imaging plays a crucial role in identifying and potentially correcting these PA reflection artifacts by identifying the acoustic reflectors responsible for them.

The Twente group recently reported on a fully integrated hand-held probe, combining an US array transducer and a diode laser module in a compact and ergonomic design that can perform dual modality US/PA imaging [36]. The probe

Fig. 8 Combined US (*gray scale*) and Photoacoustic (*red*) image showing absorption in blood vessels and the skin. (Adapted from Ref. [35]. With permission from the authors and SPIE)



consists of 128 elements, each with a length of 5 mm and a pitch of 0.245 mm. The array has a central frequency of 7.5 MHz and a measured -6 dB bandwidth of around 100 %. This dual modality probe makes use of a commercially available portable US scanner (MyLabOne, ESAOTE Europe B.V, Maastricht, the Netherlands) modified for incorporating a diode laser with a laser fluence of up to 1.3 mJ/cm^2 on the skin with an illumination spot size of $18.2 \times 2.3 \text{ mm}^2$. For PA imaging, the diode laser module was triggered using stable hardware signal from the system. This trigger signal and US transmission was controlled using system software for toggling between US and PA imaging. This system achieved a frame rate of 10 fps after averaging 20 frames during PA imaging. Line by line US measurement of the same area resulted in a screen refresh rate of 80 fps. The frame rate of this system was limited by the maximum permissible exposure (MPE) of laser light on tissue. Figure 9 shows the photograph of the portable dual modality



Fig. 9 Portable system combining ultrasound and photoacoustics. *Left* is the US scanner and *right* shows the photograph of probe combining laser module and ultrasound transducer array. (Reprinted from Ref. [36]. With permission from the authors and Optical Society of America)

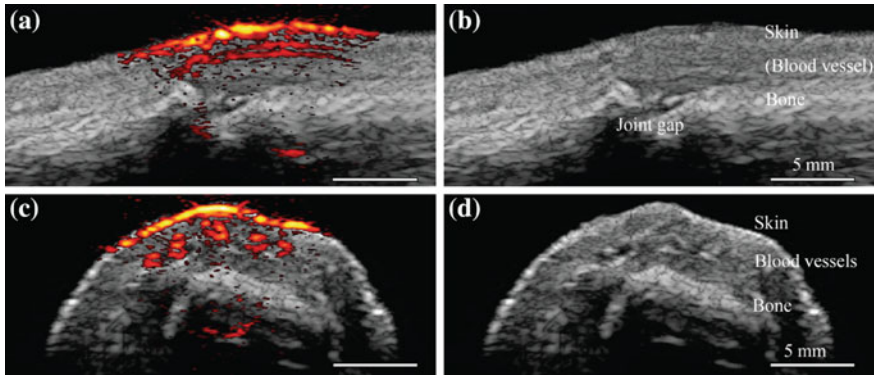


Fig. 10 Photoacoustic/ultrasound images of a human proximal interphalangeal joint in sagittal (a) and transverse (b) planes, with the *upper part* of the image corresponding to the dorsal side of the finger. On the *right side*, (b) and (c) show corresponding ultrasound only with anatomical structures indicated. (Reprinted from Ref. [36]. With permission from the authors and Optical Society of America)

US/PA system. This novel system is affordable, portable and thus undeniably a step towards clinically acceptable US/PA system.

This system was used to image a human proximal interphalangeal (PIP) joint and demonstrated detailed absorption distribution alongside the anatomical structure. Figure 10 shows combined PA/US images of the sagittal and transverse plane of the PIP. Skin, bone and joint gap are clearly visible in the US images. PA images with the complementary contrast depict the skin and blood vessel running parallel to the skin. The deeper PA signals correspond to the reflection of skin PA signal on bone. This work envisages a potential in visualizing rheumatoid arthritis using a point of care device.

2.3 The Washington University in St. Louis System

The Washington University group from St Louis in association with Philips research, North America developed a PA/US system from a commercially available US scanner [26, 28] (iU22, Philips Healthcare) which made use of a linear array probe with a bandwidth of 4–8 MHz (L8-4 Philips Healthcare). Figure 11 shows the photograph of the integrated set up.

The probe was physically integrated with a bifurcated optical fiber bundle (CB18043, Fiberguide) which was fed by a tunable dye laser (NS, Sirah) pumped by a Q-switched Nd:YAG laser (PRO-350-10, Newport). Laser pulses of 6.5 ns pulse duration were delivered for a radiant exposure of 3 mJ/cm^2 on the skin, well below the ANSI safety limit (20 mJ/cm^2).

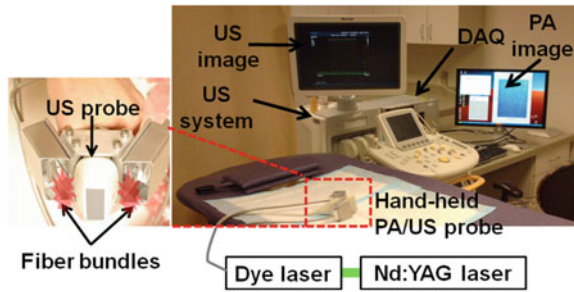


Fig. 11 Photograph of the integrated Photoacoustic (PA) and ultrasound (US) imaging system modified from a clinical US array system. (Reprinted from Ref. [26]. With permission from the authors and Optical Society of America)

The channel board in the system was modified in such a way that raw PA/US data were transferred to an external data acquisition system, which controlled the laser trigger signal, light wavelength tuning and post processing. The US images were displayed on the scanner's monitor, while the PA images, reconstructed with Fourier beam-forming, were displayed on a separate screen at 1 fps. The system was capable of frame rates up to 10 fps, but was limited due to the repetition rate of the laser (10 Hz) used.

This system proved to be effective for deep tissue imaging (5 cm) with a low radiant exposure (1/7th of the ANSI safety limit). The use of a separate data acquisition system for PA data and processing makes this system relatively expensive. Further, the US and PA images were displayed on two different screens which has implications for comparison of images in real-time.

The system was used for PA image-guided identification and needle biopsy of sentinel lymph nodes (SLN) in pre-clinical work. Imaging the axillary region in a rat before and after methylene blue injection allowed the visualization of deeply located SLN (2 cm). Figure 12a shows the control PA B-scan image in which two deeply positioned blood vessels (3.2 and 3.5 cm) are visible with excellent contrast. Figure 12b shows the image captured 10 min after the injection of methylene blue. The uptake of methylene blue in the SLN could be monitored by following the image contrast of the SLN. The overlaid PA (jet scale) and US images (gray scale) shown in Fig. 12c gives us clear morphological and functional information of methylene uptake in the SLN. The imaging depth attained without any signal averaging is comparable with the depths of axillary lymph nodes in humans (<3 cm), which shows its potential clinical utility.

The authors also showed the feasibility of imaging a biopsy needle and methylene blue intake in SLN simultaneously (Fig. 13). US imaging displayed a limited angular sensitivity for detecting a needle, as most of the incident acoustic energy is reflected away from the limited aperture US probe. Since the PA waves from the needle are cylindrical, these can be detected by the probe. PA and US image-guided SLN identification and needle biopsy demonstrated a promising substitute to

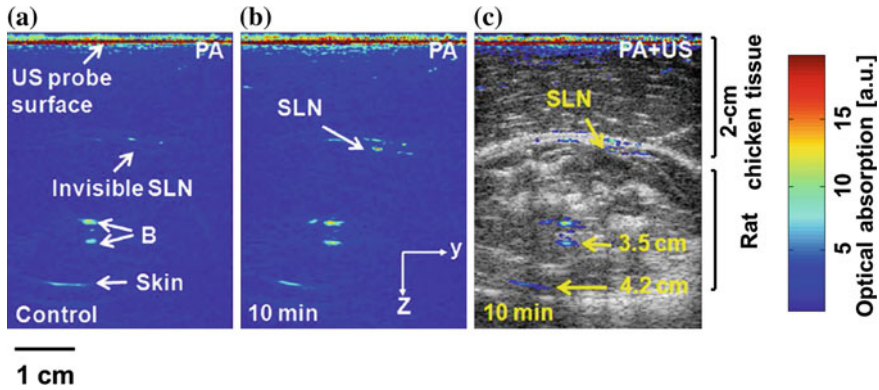
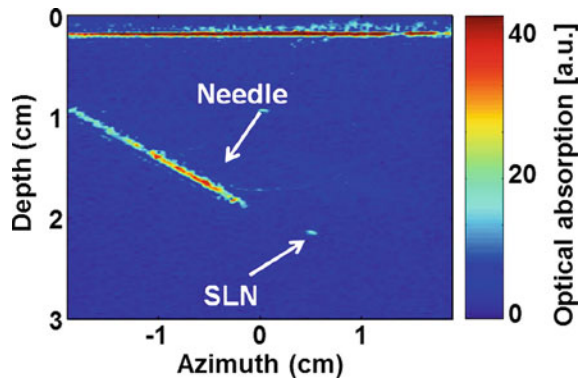


Fig. 12 In vivo deeply penetrating PA imaging. **a** Control PA image acquired before methylene blue injection. **b** PA image taken 10 min after methylene blue injection. **c** Overlaid post-injection PA (pseudo color) and US (gray scale) images. *B* blood and *SLN* sentinel lymph node. (Reprinted from Ref. [26]. With permission from the authors and Optical Society of America)

Fig. 13 In vivo PA guidance of a metal needle (18-gauge). *SLN* Sentinel lymph node. (Reprinted from Ref. [26]. With permission from the authors and Optical Society of America)



current invasive axillary staging methods for breast cancer patients. This work also demonstrated the capability of PA imaging to image deep inside tissue (5.2 cm) with laser fluence well below the ANSI safety limit (20 mJ/cm²).

2.4 The TUM (Technical University Munich) System

The group of Haisch at the Technical University Munich, developed an integrated US/PA set up (OPUS) derived from a commercial (General Electric) US scanner [37]. Figure 14 shows the schematic of the setup and US probe. A 100 Hz pulsed Nd:YAG laser pumping an OPO was synchronized with the US system that could switch between US and PA imaging. The bifurcated optical fiber (1 mm) was

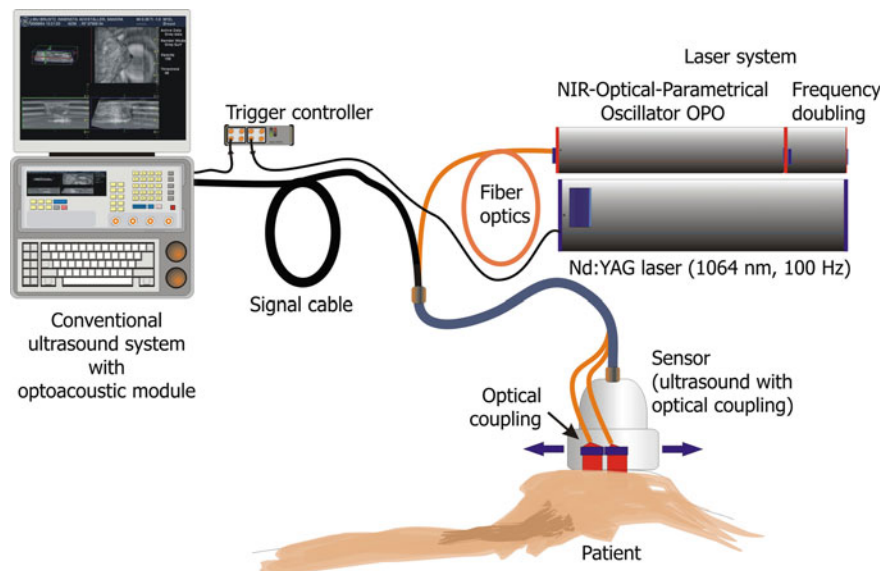


Fig. 14 Schema of setup of OPUS system. The *insert* shows the US transducer with optical coupling. (Reprinted from Ref. [37]. With permission from the authors and Journal of Analytical and Bioanalytical Chemistry)

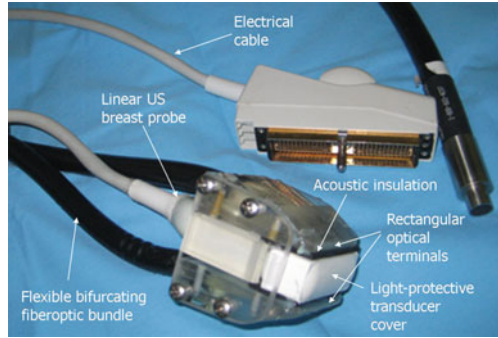
connected side by side to the US probe with a clip, which allowed for changes in illumination angle. The probe used had 192 elements with a central frequency of 8.8 MHz and a -6 dB bandwidth of 4.1 MHz. Half the elements were used for PA and other half for conventional US. The data acquisition was done here sequentially for 96 elements at the laser repetition frequency (100 Hz), which resulted in a frame rate of 1.1 fps. This system proved the ability to use an integrated US/PA system for quantitative measurements by making use of spectroscopy. They also showed that the coupling angle between the laser light and the sample surface influences the depth where a maximum PA signal is generated.

This work also compared and tested four different reconstruction algorithms [Fourier-transform-based algorithm (FTA), Hough-transform-based algorithm (HTA), delay-and sum (DnS), and circular back-projection (CBP)] on the reconstruction speed, contrast and spatial resolution of the system. However low frame rate was a bottleneck for this system to do real time in vivo measurements.

2.5 *Alpha Prototype of Imagio System (Seno Medical Instruments, San Antonio, TX)*

Fronheiser et al. [38] from Seno Medical Instruments and Fairway Medical Technologies reported a real-time laser opto-acoustic imaging system (LOIS) with

Fig. 15 Photograph of LOIS probe. (Reprinted from Ref. [38]. With permission from the authors and SPIE)



the ability to image larger blood vessels deep inside the forearm with sufficient contrast and in real-time (10 fps). Figure 15 shows the photograph of the probe used. A Q-switched Nd:YAG laser with 6 ns pulses of 1064 nm at a repetition rate of 10 Hz was used. The light coupling was achieved using a bifurcated fiber with illumination on both sides of the probe (15). The output laser beam coupled into the 12 in. randomized fiber bundle (Fiberoptics Technology, Inc., Pomfret, Connecticut) bifurcates into two rectangular beams (2×50 mm) to provide illumination with maximum radiant exposure of 15 mJ/cm^2 . This system made use of a custom-made 128-element US probe with a center frequency of 5 MHz and fractional bandwidth of 75 % focused at 20 mm using an acoustic lens. PA data was acquired and by external data acquisition system with built in amplifiers and FPGAs

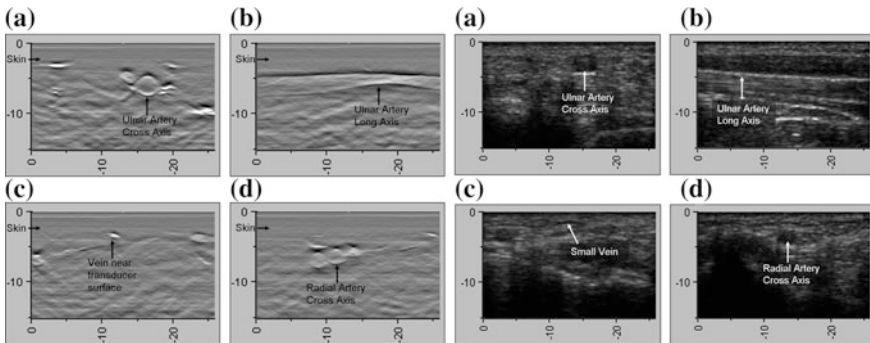


Fig. 16 PA images (left) of the wrist vessels acquired in real-time during test 1: the ulnar artery in **a** a cross axis view and **b** a long axis view, **c** a vein near the surface, and **d** the radial artery. US images (right) acquired using probe manipulations identical to those yielding PA images **a** cross axis and **b** long axis views of the ulnar artery, **c** view of a vein in the mid-wrist region, and **d** the radial artery in cross axis view. (Reprinted from Ref. [38]. With permission from the authors and SPIE)

(Field programmable Gate Arrays) for transfer to a PC. The PC-based real-time visualization of PA images was performed by custom-made LOIS-XP software that made use of 2D filtered back projection.

The authors imaged blood vessels situated deep inside the forearm using their real time (10 fps) system. The PA data in Fig. 16 (left) was sampled at 25 MHz and reconstructed at a rate of 10 fps. The US image made at the same location is also shown at right. Analysis of the cross sectional diameter of ulnary artery at higher frame rates (10 fps) opened up the possibilities to measure blood flow using this system. Change in arterial diameter clearly indicated a cyclical increase and decrease in blood volume that likely reflects the arterial blood flow. This suggests that a real-time PA system can potentially be used, similarly to photoplethysmography, for monitoring blood flow.

2.6 *The University of Arizona System*

Appropriate light delivery has been an issue in PA imaging using commercial US scanners. In most of the systems explained above, light enters tissue at oblique angles and intersects the imaging plane in the tissue. This geometry confines the illumination pattern to specific depths, which is not optimal for imaging the entire region of interest. To address this issue, Montilla et al. [39] came up with a solution called PA enabling device (PED) which can be hooked to any linear array US probe.

The approach exploits an optically transparent acoustic reflector to help direct laser illumination to the region of interest. PED was demonstrated in a system where the source is a pulsed laser coupled to an optical parametric oscillator (Surelite™ 532 nm I-20 and OPO plus; Continuum, Santa Clara, CA), producing wavelength tunable pulses at 20 Hz. Light was coupled to the PED using an optical fiber (CeramOptec, East Longmeadow, MA). The US scanner used was a commercially available one (z.one Zonare Medical Systems) connected to a 64 elements linear array probe (7.5 MHz). Frame rates of 20 fps were achieved for PA imaging, which was limited by PRF of the laser. US imaging was done using plane-wave transmission and beam-forming. US and PA data from the scanner were transferred to a PC using Ethernet interface. Reconstruction was performed in MATLAB (Mathworks, Natick, MA) using delay and sum beam-forming considering one way (PA) or two-way propagation (US) of the acoustic waves. Figure 17 shows the mechanism of connecting PED to probes and how light illumination and collection of PA signals can be improved. Figure 18 shows the use of PED along with a linear array probe and a photograph of a live measurement.

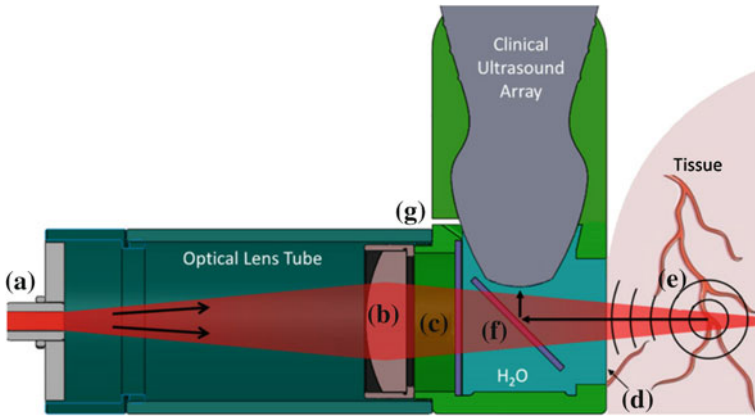


Fig. 17 Cross-sectional view of the PA enabling device (PED) design as an attachment to a clinical ultrasound probe. **a** Fiber optic connector, **b** cylindrical focusing lens, **c** glass window, **d** thin transparent membrane, **e** optical absorbers, **f** reflecting glass plate, **g** drain hole. (Reprinted from Ref. [39]. With permission from the authors and IOP Publishing)

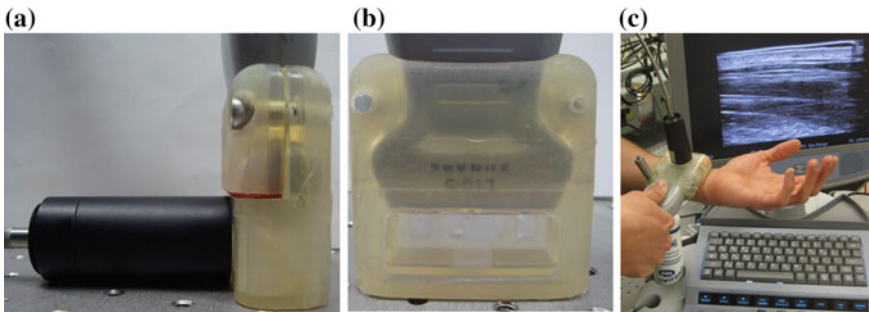


Fig. 18 **a** and **b** Photograph of Liner array probe connected to PED. **c** Photograph of the integrated system during imaging of wrist. (Adapted from Ref. [39]. With permission from the authors and IOP Publishing)

2.7 The Helmholtz Zentrum/Technische Universität München Systems—Ntziachristos Group

From the group of Ntziachristos at the Technical University Munich, Buehler et al. [40] developed a real-time handheld multispectral optoacoustic imaging system (MSOT). Although this novel video-rate handheld system does not have US imaging capability (not reported), it is included in this review for showing the clinical relevance of multi-spectral photoacoustic imaging. Figure 19 shows the details of the handheld probe. This system used a fast laser compared to the previous MSOT system reported by the same group. The fast operation and switching

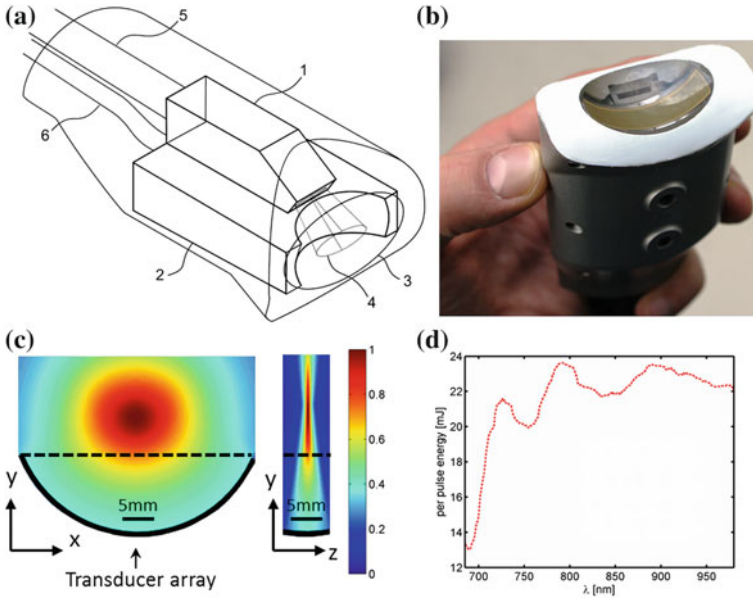


Fig. 19 Drawing of the handheld device (a) and photograph of it (b). Simulated sensitivity distribution of the array within the detection band (c) and the wavelength dependency of the laser energy (d). 1 Fiber bundle output; 2 transducer array; 3 membrane; 4 illumination pattern; 5 fiber bundle, 6 electrical cables. (Reprinted from Ref. [40]. With permission from the authors and Optical Society of America)

of wavelengths helped in motion insensitive measurements, which is very crucial for systems based on handheld probes.

The US probe used was a custom made array of 128 elements with center frequency of 8 MHz and transmit-receive bandwidth of 60 % manufactured using 1–3 piezo-composite technology. The elements in this probe were arranged in one row forming a spherical concave array. Light illumination was provided by a custom built laser system based on an OPO (680–980 nm) and pumped with a diode pumped Nd:YAG laser (InnoLas Laser GmbH, Krailing) which generated laser pulses with duration less than 10 ns and with a repetition rate of 50 Hz which helped in real time imaging. Light was coupled into a custom silica fused-end fiber bundle consisting of 256 fibers. At the output side of the bundle, the fibers were arranged in a rectangular aperture of dimensions 2 mm \times 2 mm. It serves to create an illumination zone of \sim 2.5 mm height and \sim 12 mm width on the surface of the subject, coinciding with the US detection plane. The data acquisition system used here also was custom made which provided the capability of acquiring data from all 128 channels simultaneously. Signal processing, image reconstruction and spectral unmixing were performed on the GPU of the computer in real time. The coupling of tissue and probe was done in a novel way by making use of an acoustically transparent membrane, creating a cavity between it and the transducer array surface

that was filled with water for good coupling of US. The authors also demonstrated the use of a model based inversion technique for better reconstruction of PA images.

This handheld Multispectral optoacoustic Tomography (MSOT) system was used to demonstrate the capability of differentiating between arteries, veins, and melanin based on their known absorption spectra. Figure 20a, b show the PA image of the left wrist of a healthy volunteer with wavelength 760 and 860 nm respectively. Figure 20c shows the spectral profiles of the marked points in Fig. 20b. Spectrum 1 strongly resembles the absorption spectrum of melanin; spectra 2, 3, 4, and 5 resemble deoxyhemoglobin with its characteristic peak at 760 nm, and spectrum 6 resembles the absorption of oxyhemoglobin.

The authors also demonstrated dynamic imaging by obstructing and releasing the blood flow to the finger of a healthy volunteer and monitoring the changes using multispectral PA imaging. By this, they were able to extract temporal evolution of oxy and deoxyhemoglobin, total blood volume ($BV = [Hb] + [HbO_2]$) and the oxygen saturation ($SaO_2 = [HbO_2]/BV$) dynamically.

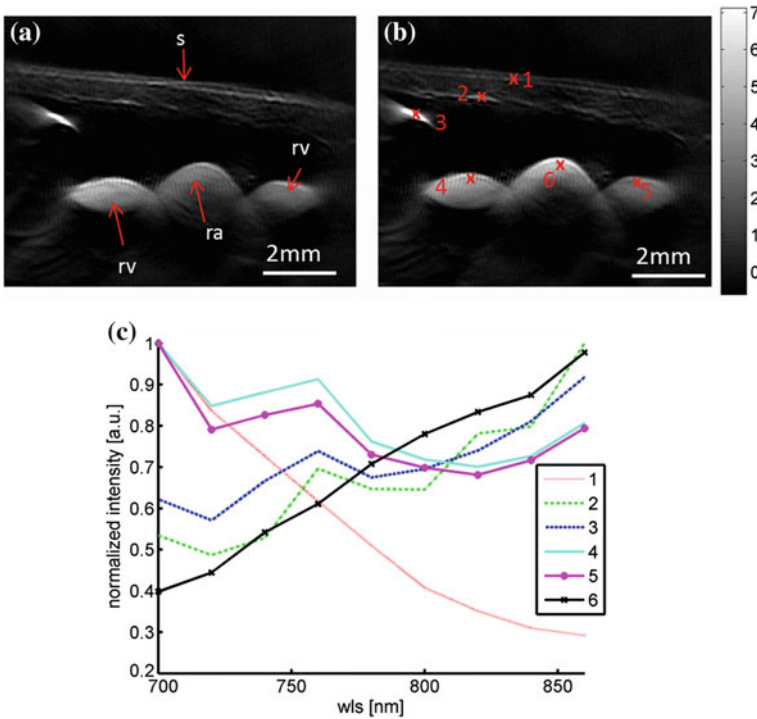


Fig. 20 **a** Photoacoustic image of the wrist at 760 nm and **b** 860 nm. *rv* Radial vein; *ra* radial artery; *s* skin. **c** Profiles through the multispectral dataset from the locations labeled in (b). (Reprinted from Ref. [40]. With permission from the authors and Optical Society of America)

Figure 21a, b shows the unmixed deoxyhemoglobin signal, superimposed onto the total BV image, 10 s before (Fig. 21a) and 15 s after (Fig. 21b) release of the rubber band used for obstructing blood flow. Figure 21c, d show the corresponding oxyhemoglobin signal. Figure 21e depicts the temporal evolution within the area marked in Fig. 21c during the measurement time. The accumulation of deoxygenated hemoglobin, when the blood flow was obstructed is evidently visible as higher signal just below the skin (Fig. 21a). This signal got diminished once the blood flow was normal (Fig. 21b).

Dima et al. [41] from the same group reported dual mode PA/Duplex ultrasound (DUS) measurements of the carotid artery at the peak of volumetric expansion caused by heartbeat in a healthy volunteer. DUS is a combination of conventional anatomical US and color Doppler US. This work makes use of a different system with custom made curved array US probe (64 elements, 5 MHz center frequency).

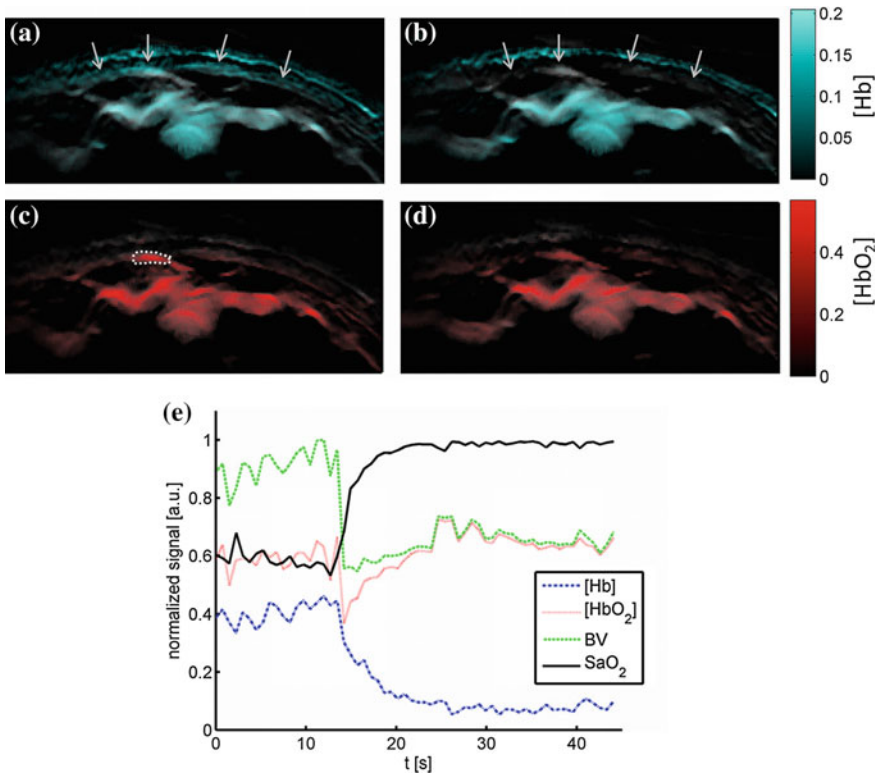


Fig. 21 a–d Unmixed deoxyhemoglobin (Hb) and oxyhemoglobin (HbO₂) superimposed onto the total BV image before (*first column*) and after (*second column*) release of vascular blocking. **e** Temporal evolution of the extracted properties within the area indicated in (c). The *arrows* indicate the area at which the deoxyhemoglobin signal changes. (Reprinted from Ref. [40]. With permission from the authors and Optical Society of America)

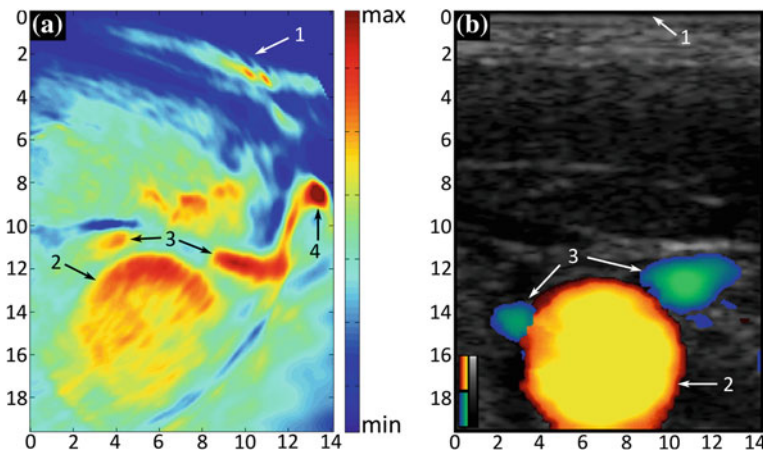


Fig. 22 Carotid imaging using photoacoustics and duplex ultrasound. **a** Photoacoustic image, **b** Directional DUS image indicating positive flow in *yellow/red*; negative flow in *green/blue*. 1 Skin surface, 2 common carotid, 3 internal jugular vein, 4 external jugular vein. (Reprinted from Ref. [41]. With permission from the authors and Optical Society of America)

Figure 22a shows the PA image acquired at a wavelength of 800 nm. The common carotid artery is visualized (marked as 2) clearly as a round structure from depth of 12–18 mm. The skin (marked as 1), the right internal jugular vein (marked as 3) and an external jugular vein (marked as 4) are also visible in the image. To validate the findings, DUS of the same location was also performed (Fig. 22b). The color maps used (positive flow: yellow/red; negative flow: green/blue) simplify identification of the carotid artery and vein. The linear array used for DUS measurement here flattened the skin and pushed the external jugular vein out of the imaging window. Because of less pressure applied when holding the probe, the common carotid is seen at slightly a different depth (13–19 mm). The right internal jugular is also visible in the DUS image. This demonstrated that PA imaging could be a good complementary technique along with DUS for imaging Carotid and surrounding vascular structures.

2.8 The Helmholtz Zentrum/Technische Universität München Systems—Razansky Group

From the group of Razansky at the Technical University Munich, Dean-Ben et al. [42] reported on the development of a portable clinical system for three dimensional photoacoustic visualization of deep human tissues at video rate. Three-dimensional PA imaging and spectroscopy using a handheld probe, without any cumbersome scanning stage was a novelty. This system without US imaging capability (not reported) is included in this review because of its innovative probe design and

capabilities. This vMSOT (Volumetric Multi-spectral opto-acoustic tomography) device used a custom made two-dimensional array of 256 ultrasonic detectors (Imasonic SaS Voray, France) arranged upon a spherical surface with a radius of 40 mm and covering a solid angle of 90° . Elements had a center frequency of 4 MHz and a bandwidth of 100 %. Figure 23a, b show the layout and photograph of the probe respectively. The elements were manufactured using piezo-composite material for better sensitivity. This is important for real time imaging as improving SNRs by averaging is not the best option.

The arrangement of transducer elements here helped in allowing a full tomographic access to the area of interest by collection of signals from broad angles. The excitation light from a pulsed laser was delivered to the object through a silica fused-end fiber bundle (CeramOptics GmbH, Bonn, Germany) inserted into a hole located in the center of detection array as shown in Fig. 23a. A wavelength tunable (690–900 nm) optical parametric oscillator (OPO) laser (Phocus, Oportek Inc; Carlsbad, CA) generating 10 ns pulses at a repetition rate of 10 Hz was used. Raw data from all elements were simultaneously sampled at 40 MHz and using a custom made data acquisition system (Falkenstein Mikrosysteme GmbH, Taufkirchen, Germany). The acquired data were then reconstructed on a workstation computer 2x Intel Xeon DP X5650 (6×2.67 GHz) with 144 GB of RAM. Since one laser pulse could produce complete volumetric data sets from imaged object, 3D real time imaging was possible with this system.

The system while claiming excellent resolutions with many capabilities uses custom-made components such as the US probe, data acquisition system, computer and the laser, which would make it quite expensive. The repetition rate of the laser (10 Hz) limited the time resolution of this system.

The authors demonstrated high resolution volumetric multispectral photoacoustic tomography for real-time visualization of blood oxygenation parameters. This

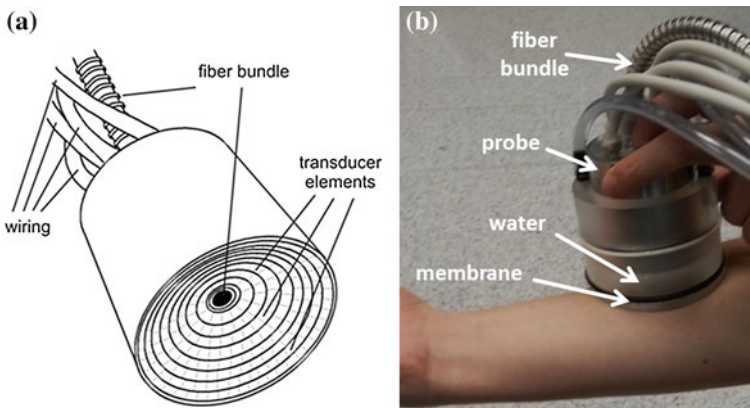


Fig. 23 **a** Layout of the probe showing the arrangement of transducer elements and fiber bundle. **b** Photograph of the probe during measurement. (Reprinted from Ref. [42]. With permission from the authors and Elsevier)

work claimed the capability to do three dimensional real time imaging with the handheld probe, which is evidently difficult to achieve using other imaging devices.

Figure 24 shows the results of multispectral tomographic imaging of the wrist of a healthy volunteer. It is clear from Fig. 24a that pixel intensity increases with wavelength for some of the vessels (Arteries) and it remains more or less constant for other vessels (Veins). Strongest background signal was observed for 700 nm as melanin absorbs more at this wavelength. By applying a spectral unmixing algorithm, map of blood oxygenation (Fig. 24b) accurately revealed the location of veins and arteries. This work has good potential as a clinical tool, particularly in applications related to cardio vascular diseases, where blood oxygenation and delivery are diagnostically critical.

The same group recently reported an improved version of this system which used a fast laser with fast wavelength tuning which in turn provide volumetric spectrally enriched tomography in real-time [43]. Figure 25 shows the schematic representation of this handheld photoacoustic-imaging scanner. This is the first reported system which delivers feasibility of PA imaging in 5 dimensions, i.e., rendering volumetric images of spectrally resolved photoacoustic data in real time. The US array used was the same as in their previous system [42]. The illumination source was a custom-made optical parametric oscillator-based laser, generating 5 ns duration pulses with energy of up to 20 mJ at a pulse repetition rate of up to 50 Hz.

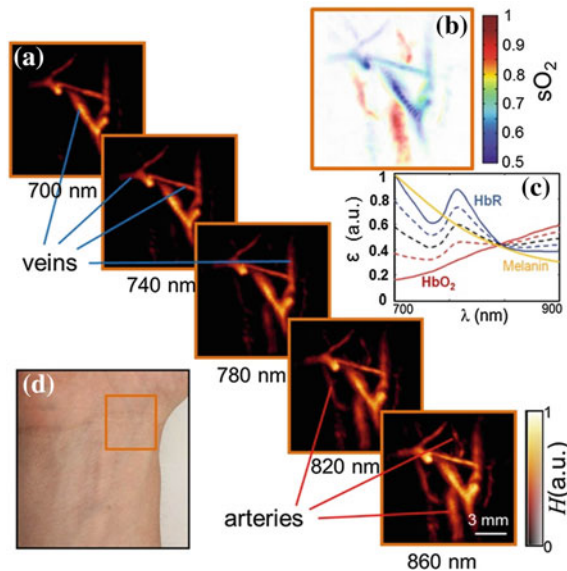
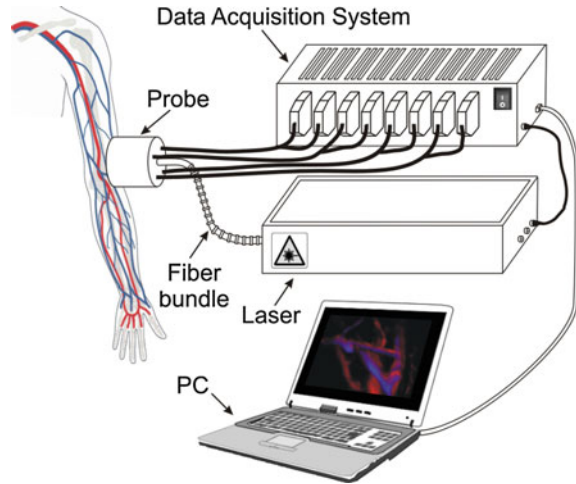


Fig. 24 Multispectral tomographic reconstructions of the wrist region. **a** Volumetric images acquired at 5 different wavelengths in the near infrared. **b** Map of blood oxygenation saturation as calculated from images acquired at different wavelengths. **c** Absorption spectra of major tissue chromophores in arbitrary units. **d** Color photograph of the imaged region. (Reprinted from Ref. [42]. With permission from the authors and Elsevier)

Fig. 25 Schematics of the real-time handheld optoacoustic imager. (Reprinted from Ref. [43]. With permission from the authors and Nature Publishing Group)



A dedicated tuning system based on fast mechanical rotation of the optical parametric oscillator crystal had been developed that allowed changing the wavelength to any value between 700 and 900 nm on a per-pulse basis. In this way, only 100 ms was required to acquire an entire volumetric multispectral dataset at five different wavelengths. The acquired data was then transferred to a personal computer using Ethernet port and GPU based processing was done. A 3D back projection reconstruction algorithm with spectral un-mixing for spectral analysis, could be performed by the GPU enabled system in less than 20 ms. The fast acquisition, switching of wavelengths and processing helped to provide truly real time multi-spectral tomographic imaging. This state of the art system opens new prospects with several important clinical applications envisioned in clinical practice as well as in pre-clinical research. The only limitation of this system to enter the clinics would be the bulky laser used for the purpose.

2.9 The VisualSonics System

Needles et al. [44] reported on the development and initial application of a fully integrated PA micro-US system, which offered co-registered US and PA imaging with options for spectral measurements. Figure 26 shows the schematic diagram of the prototype Photoacoustic imaging system (Vevo LAZR, VisualSonics, Toronto, ON, Canada) developed by them.

The US probe used in this system was a linear array probe (MS250, VisualSonics Inc) having 256 elements with a center frequency of 21 MHz. Light illumination was provided by a tunable (680–970 nm) NIR Nd:YAG laser with a repetition rate of 20 Hz. The light was coupled using fiber optic bundles to the special housing where the US probe was fixed in such a way that crossed laser beam

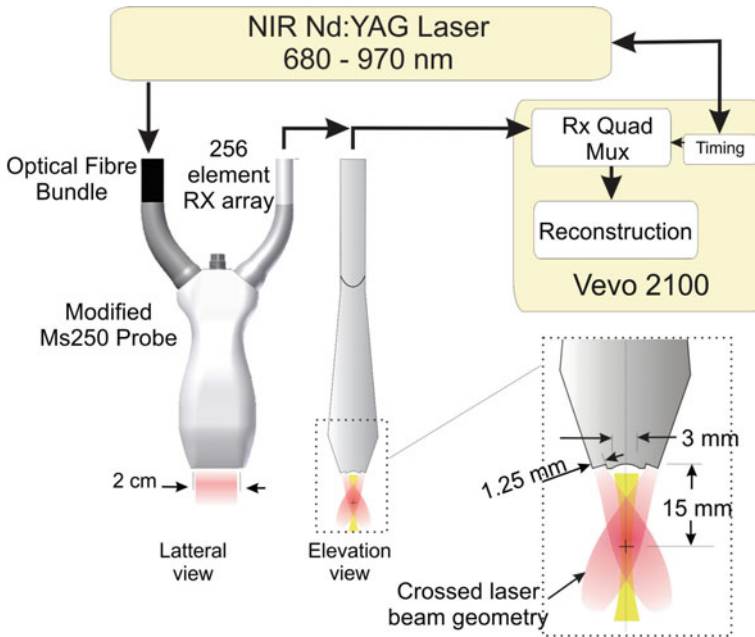


Fig. 26 Schematic diagram of the LAZR photoacoustic imaging system showing (left) the integrated transducer array and the block diagram of the signal processing chain. Separate cable/fiber-optic bundles are used to excite optical and or acoustic elements (right). (Reprinted from Ref. [44]. With permission from the authors and IEEE)

geometry at around 15 mm deep was achieved as shown in Fig. 26. On receive, signals from 4 blocks of 64 elements (256 total) were transferred back to the Vevo 2100 scanner for reconstruction of a full-frame PA image. The laser repetition rate used here was 20 Hz, yielding a PA imaging rate of 5 Hz. Screen interfaces allowed the user to select wavelengths in the 680–970 nm range or to select an oxygenation mode in which sequential PA frames were acquired at 750 and 850 nm to calculate total hemoglobin and oxygen saturation. Three-dimensional data were acquired by scanning the transducer using a linear stepper motor during 2D PA measurements.

The system is intended predominantly for pre-clinical work such as visualizing and monitoring vasculature associated with cancer growth in small animals such as mice. Clinical applications are not impossible with the instrument, but with the present high-frequency US probe these will be restricted to superficial imaging applications. The laser used here was again bulky in the present version.

Langhout et al. [45] used this system from Visualsonics and showed the viability of using PA imaging to identify melanoma metastasis in human lymph nodes. Multispectral Photoacoustic Imaging with spectral unmixing was employed for required contrast. High-resolution US imaging was also done for orientation and identification of structures.

This work was able to differentiate optical absorption by melanin and hemoglobin in resected human lymph nodes by careful selection of light wavelength. Figure 27a shows the US image of a tumor positive lymph node. Here the node is seen as a round structure, surrounded by hyperechogenic fat tissues. The corresponding PA image (Fig. 27b) shows strong surface signals, while deeper within the node signals are absent. Spectral unmixing was performed to confirm the reason for the high contrast region in PA image. The resulting image superimposed on the US image is shown in Fig. 27c, where the green region represents pixels with spectral resemblance to melanin. The presence of the high absorbing melanin deposits at the surface limited light penetration to a few mm leading to the lack of signal from deeper within the node. There appear no traces of blood contrast from the spectral unmixing in this region, and this observation is validated from histopathological findings.

Figure 27d shows the US image of a benign lymph node. This shows a bean shaped node with a brighter hilum enclosed by bright fatty tissue. The PA image (Fig. 27e) displays vessel-shaped structures at 16 mm depth and signal at the surface of the fatty tissue. Spectral unmixing and analysis (Fig. 27f) indicate that the vessels shaped structures contain blood, while the signal from the surface of the fatty regions does not resemble either the blood or melanin reference spectra. This work shows the relevance of combining the two modalities, with a complete anatomical visualization of the node using US, combined with the spectroscopic molecular selectivity possible with PA.

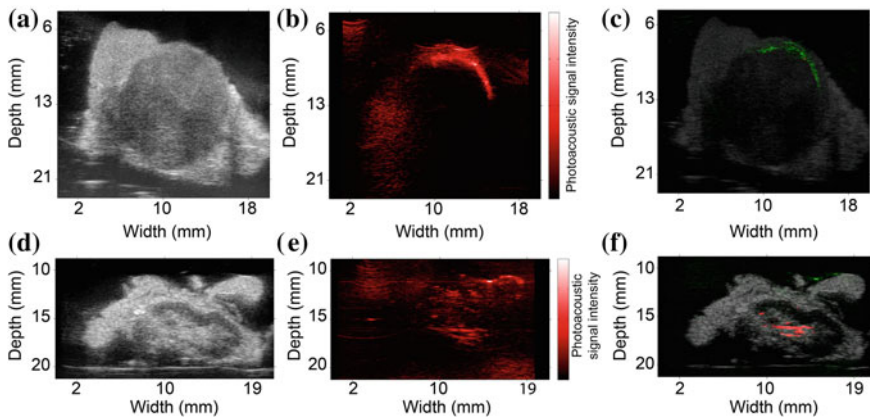


Fig. 27 Photoacoustic imaging (Ex Vivo) of human Lymph Nodes: Tumor positive node images (a, b, c), Benign node images (d, e, f); a and d Ultrasound image, b and e Photoacoustic image, c and f Spectrally unmixed PA image superimposed on ultrasound image. (Adapted from Ref. [45]. With permission from the authors and Hindawi Publishing Corporation)

2.10 The University of Michigan Systems

From the group of Wang, Yuan et al. [46] reported on a real-time integrated US/PA system in which back-projection (BP) algorithm for PA image reconstruction was optimized to reduce the computational cost and facilitate parallel computation on a state of the art graphics processing unit (GPU) card. For building this system, the Verasonics US Data Acquisition platform (Model V3, Redmond, WA) was programmed to work along with the multicore computer equipped with the NVidia GeForce GTX690 GPU card. The US probe used here was a linear array probe (CL15-7, Philips North America Corporation, Andover, MA) with 128 elements, 11.25 MHz center frequency, and a 75 % -6 dB bandwidth. The illumination was provided by a tunable optical parametric oscillator (OPO) (Vibrant B, Oportek inc; Carlsbad, CA) pumped by the second harmonic output of a Nd:YAG pulsed laser (Brilliant B, Quantel, Bozeman, MT). Laser pulse duration and pulse repetition frequency are 5.5 ns and 10 Hz respectively. By switching the transmission on and off, exactly synchronized with the laser pulses, this system employed the PA and US modes alternatively, both at a frame rate of 10 Hz. The PA and US

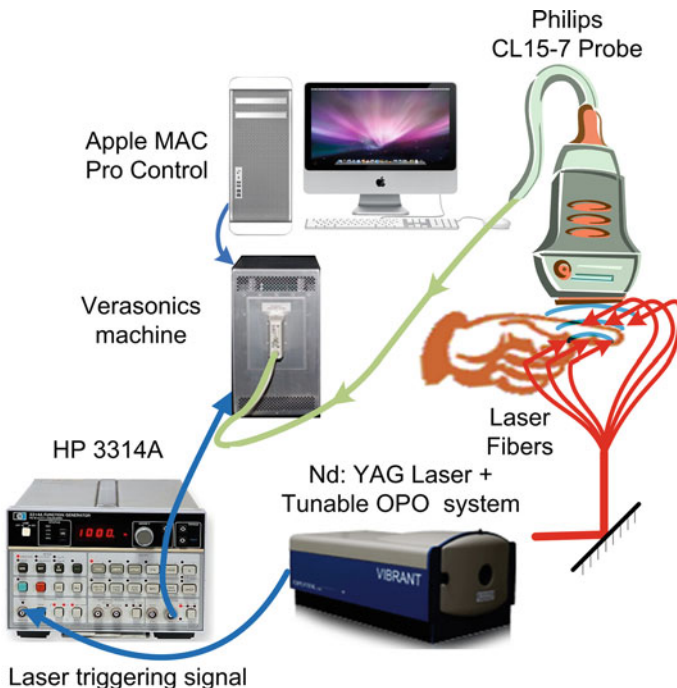


Fig. 28 Schematic diagram of the real-time US/PA system. (Reprinted from Ref. [46]. With permission from the authors and SPIE)

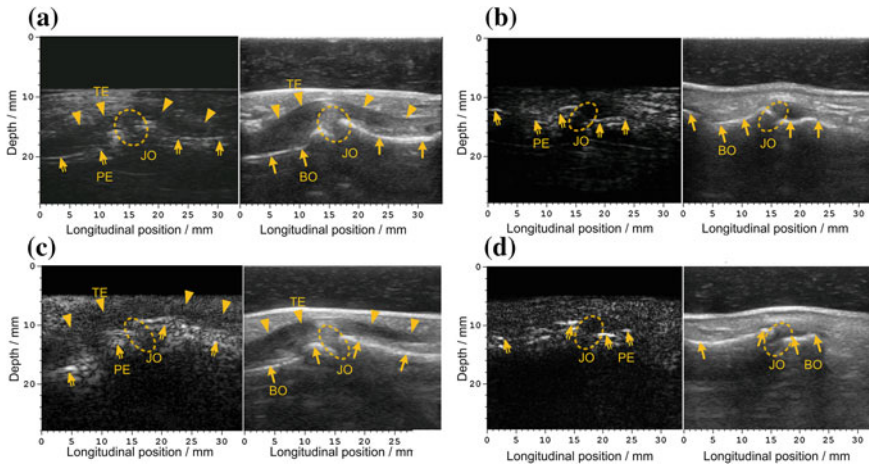


Fig. 29 PA (left in each subfigure) and US (right in each subfigure) images acquired from healthy volunteers. **a** Coronal plane [volar] and **b** sagittal plane images acquired from the PIP joint of an index finger of a male volunteer; **c** Coronal plane [volar] and **d** sagittal plane images acquired from the PIP joint of an index finger of a female volunteer. *TE* Tendon, *JO* joint, *PE* periosteum, *BO* bone. (Reprinted from Ref. [47]. With permission from the authors and SPIE)

measurements were done alternatively and displayed on the same screen at a rate of 10 fps. US image processing and reconstruction was performed on the multicore CPU, while PA image reconstruction was completely done on the GPU, avoiding conflicts between processing and display of the two imaging modes. Figure 28 shows the schematic of the system.

In PA imaging mode, when the image size was 1024×512 pixels and the data volume of signals was 128 channels by 2048 points, the maximum frame rate achieved with this system was 17 fps, sufficient for visually continuous real-time imaging. This real time US/PA system was found to be promising for clinical settings except for the fact that it makes use of a bulky water-cooled Q-switched laser system.

Xu et al. [47] from the same group imaged finger joints with a slightly different version [not real-time] of PA/US system and demonstrated the ability to recover comparable features using both contrasts in healthy finger joints being able to depict the osseous structures, as well as tendon and cartilage (Fig. 29). However, the US images represent backscattered acoustic energy from bony structures, while PA images most likely represent optical absorption in the vasculature at the bone surfaces. For the first time, it was shown that the tendon could be distinguished compared to the surrounding soft tissue in PA images primarily based on the higher blood content in the latter. This work shows that NIR light penetration is sufficiently deep for PA B-scan imaging of finger joints, which may have potential in visualization of inflammation in rheumatoid arthritis.

2.11 The Acoustic Delay-Line System

Cho et al. [48, 49] recently reported on a handheld PA tomography probe built using acoustic delay lines. Figure 30b shows the basic principle employed in this system in comparison with the traditional systems (Fig. 30a). This system was not capable of US imaging, but the technique used is worth reviewing considering the novelty in it, which envisages miniaturized systems for PA tomography. The typical propagation time of a PA signal in the tissue is in the range of microseconds (μs), while the time between generation of two PA signals is much longer, typically of the order of milliseconds (ms), depending on the laser repetition rate (10–20 Hz). The system proposed here made use of this knowledge to delay the PA signals from different channels and acquire using two transducers instead of an array. This simplified the set up and reduces the overhead of using data acquisition systems that could handle multiple channels at a time.

The experimental setup is shown in Fig. 30c. The light source used was a frequency doubled Q switched Nd:YAG laser (Continuum, SL2-10, San Jose, California) with a pulse duration of 5 ns, repetition rate of 10 Hz and wavelength of 532 nm. The PA waves generated were passed through the optical fiber PADL probe for adding required delay and acquired by two DAQ channels. In each DAQ channel, eight time delayed PA signals were sequentially detected by a single element unfocussed US transducer (Olympus NDT, V303). Detected signals were then averaged 10 times to generate images at a frame rate of 1 fps. The concept reported here was novel and handy for making the size of systems small and inexpensive. It could receive signals from 16 channels by just making use of 2 US detectors and two DAQ channels, which corresponded to a channel reduction ratio of 8:1. But the application of this method in vivo is far from reality as lateral resolution depends on number of PADL's in use. It is practically difficult as of now to build complex probes with large number of PADLs with outsized length.

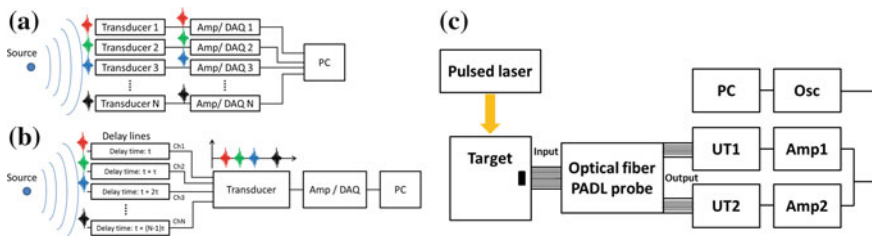


Fig. 30 a Photoacoustic signal reception using conventional way (Multiple detectors and multi-channel DAQ). b PA signal reception using acoustic delay lines (Single element transducer and single channel DAQ). c Experimental set up using 16-channel PADL probe. (Reprinted from Ref. [49]. With permission from the authors and SPIE)

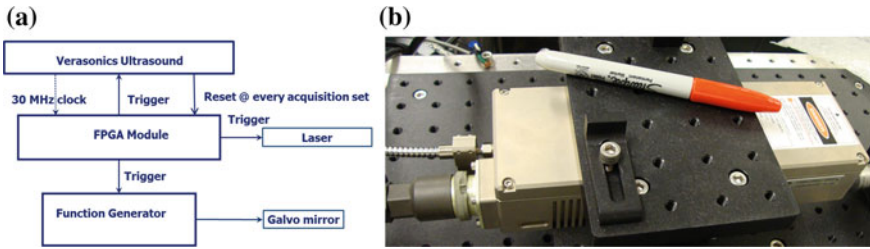


Fig. 31 **a** Block diagram of integrated US/PA system, including a FPGA module. **b** Photograph of the used diode pumped laser system. (Adapted from Ref. [14]. With permission from the authors and SPIE)

2.12 The University of Washington System

Xia et al. [14] recently reported on a system which they describe as being translational, and which is claimed to be a step for making US/PA dual mode imaging clinically acceptable. The expensive and bulky laser with low repetition rates (10–20 Hz) has been one of the main limitations of current research systems aiming at real-time PA imaging for patient use. This integrated US/PA system avoids these limitations by making use of a portable, low-cost, low pulse-energy fiber laser (HM 40 W G3.1, SPI, South Hampton, UK), with repetition rates as high as 100 kHz. The laser system used is shown in Fig. 31b. This is claimed to be potentially the next generation of light sources for real time PA imaging systems.

The low pulse energy around 1 mJ/pulse at 1064 nm, requires a small spot of 1–2 mm diameter, which results in shallow penetration depths. To improve on this, the system uses fast spot scanning using a scanning galvo mirror (GVS001, Thorlabs, Newton, NJ, USA) to form a final synthesized PA image from single shot PA images. The system was built around the Verasonics (Verasonics, Redmond, WA, USA) US platform. The US transducer was a linear array probe with 64 elements (AT8L12-5 50 mm, Broadband, Hsinchu, Taiwan), for both US and PA imaging. An FPGA module synchronized the US system and the galvo mirror based on the clock signal from US system. Figure 31a shows the control block diagram of the system. Over an imaging field of $2\text{ cm} \times 1\text{ cm}$, a combined frame rate of 32.8 Hz for both PA and US was achieved which is remarkable. The frame rate here could be improved by increasing the number of transducer elements and simultaneously acquiring data.

2.13 The University of Texas System

Shah et al. [50] reported the feasibility of using PA imaging to detect photoabsorbers and to monitor temperature during photothermal therapy. To perform

Fig. 32 Experimental setup for photoacoustic and ultrasound imaging during therapy. (Reprinted from Ref. [50]. With permission from the authors and SPIE)

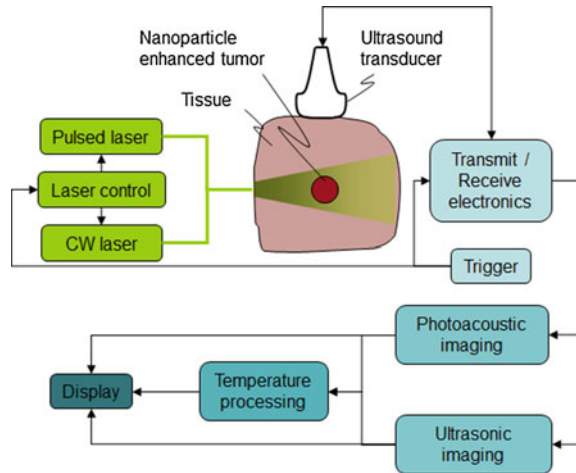


image-guided therapy, a laboratory prototype of a PA and US imaging system, consisting of a pulsed laser and an array-based US imaging system, was interfaced with a continuous wave therapeutic laser. This work is included in the review to showcase the promising application of image guided therapy using dual modality US/PA system. They integrated imaging and therapy system to acquire PA and US frames during photothermal therapy. Figure 32 shows the schematic of the experimental set-up.

A 128 element linear array transducer, with element spacing of about 300 μm , (SonixRP, Ultrasonix Medical Corporation, Canada) was used to capture US pulse-echo and PA data. The signals were logged using a 40 MHz sampling rate. The nominal center frequency of the transducer in the pulse-echo regime was 5 MHz. An OPO pulsed laser system (Vibrant B, Opotek Incorporated, USA) operating at an 800 nm wavelength, with a 5 ns pulse duration and a 10 Hz repetition rate providing optical fluence up to 15 mJ/cm^2 was interfaced for PA imaging. A continuous wave diode laser (HAM, Power Technology, Incorporated, USA), operating at 800 nm with a maximum power of 1 W, was used as a light source for the photothermal therapy.

The authors performed photothermal therapy experiment on porcine tissue with injected photoabsorbers for proving the feasibility of using PA/US imaging for guidance and monitoring during therapy. US based thermal imaging utilized thermally induced speckle motion and PA based temperature measurement relied on temperature-induced amplitude variations in PA signal. PA and US techniques were compared for their sensitivity to monitor temperature changes during the therapy. PA based thermal imaging was found to be having higher CNR (Contrast to noise ratio) when compared to US thermal imaging. Figure 33a, b show the US and PA image of the region respectively. The site of the photoabsorber injection is indicated by the dashed circle in the US image, which also corresponds to the location of the

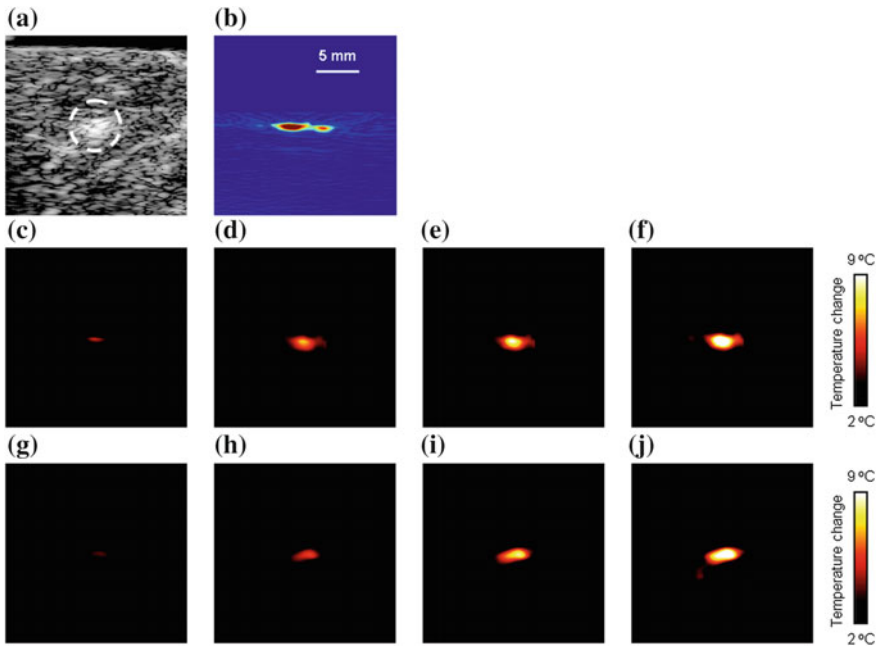


Fig. 33 Photothermal therapy experiment on porcine tissue with injected photoabsorbers. **a** Initial ultrasound and **b** Photoacoustic images. The injection site is marked by a *dashed circle* in the ultrasound image. **c–f** Photoacoustic-based thermal images and **g–j** ultrasound-based thermal images after 60, 120, 180, and 240 s of therapy. All images cover a 20×20 mm field of view. (Reprinted from Ref. [50]. With permission from the authors and SPIE)

strong PA response. For comparison, both US and PA imaging are used for thermal imaging. Figure 33c–f show the PA based thermal images and Fig. 33g–j show the US based thermal images. This Ex vivo tissue study indicates that PA and US thermal imaging can be used together to compute temperature change during photothermal therapy with high sensitivity and good SNR throughout the imaging volume. Ke et al. [51] recently reported that it is possible to measure the spatial distribution of temperature in deep tissue using PA imaging with a precision of -0.8 ± 0.4 °C (mean \pm standard error). Since lot of clinically approved photoabsorbers for thermal therapy are available, future of PA/US based thermal imaging is bright.

Table 1 summarizes the characteristics of all important handheld probe-based dual mode US/PA imaging systems reported in recent years. A few systems without US imaging capability are also included to show different technical advancements and applications.

Table 1 Comparison of different handheld probe based PA/US systems

Research group (Published year) [References]	No of probe elements	Center frequency (MHz)	Bandwidth (-6 dB) (%)	US imaging capability	Laser wavelength	Laser pulse repetition frequency (PRF) (Hz)	Frame rate (Hz)
Niederhauer et al. (2005) [27]	64	7.5	76	Yes	760 nm	7.5	7.5
Kolkman et al. (2008) [35]	128	7.5	75	Yes	1064 nm	1000	8
Kim et al. (2010) [26]	128	6	67	Yes	Tunable dye	10	1
Haisch et al. (2010) [37]	96(192)	8.8	50	Yes	OPO	100	1.1
Fronheiser et al. (2010) [38]	128	5	75	No	1064 nm	10	10
Montilla et al. (2013) [39]	64	≈7.5	≈67	Yes	OPO	20	20
Buehler et al. (2013) [40]	128	8	60	No	OPO	50	50
Dean-Ben et al. (2014) [43]	256	4	100	No	OPO	50	≈50
Needles et al. (2013) [44]	256	21	52	Yes	OPO	20	5
Yuan et al. (2013) [46]	128	11.25	75	Yes	OPO	10	10
Xia et al. (2014) [14]	64	≈10	≈70	Yes	1064 nm	1000	32
Daoudi et al. (2014) [36]	128	7.5	100	Yes	800 nm	1000	10

3 Concluding Remarks, Envisioned Improvements and Applications

A PA imaging set-up consists of a laser illumination system attached to an US detector array and a data acquisition system for acquiring US signals. Commercially available US probes are not specifically designed to be sensitive for PA signal transduction. The relatively low amplitudes and wide frequency bands of PA signals call for custom-made sensitive and wide bandwidth transducers as receivers [52, 53] for PA imaging, which may not be appropriate for US imaging. In case of dual modality US/PA system, the selection of available commercial US probes is a compromise. Novel US probes with enhanced sensitivity and noise performance suitable for PA/US imaging are reported [54], but still in research stage. Commercial probes are centered around frequencies typically between 7.5 and 12 MHz, and possessing bandwidths under 80 %. This limits the sizes of objects that can be faithfully reconstructed to sub-mm sized structures.

Another key aspect of a PA/US system is the light delivery scheme. For deeper relevant penetration depths, high power Q-switched lasers are required which are typically expensive and bulky. These may not be suitable for a clinical setting. All the systems reviewed here excepting Ref. [14, 36] use bulky laser systems, even if the probes are handheld and compact. To maintain the portability of the US equipment, it is important to device handy and compact light sources that can provide reasonable energy for deep PA imaging. Another crucial element to be considered is the frame rate of the system, which is in turn dependent on the repetition rate of the laser. A Q-switched Nd:YAG laser commonly used for PA imaging have pulse repetition frequency (PRF) of ten to hundreds of Hertz [55]. This limits the time resolution of the system. There are developments in this field and fast lasers capable of PRF up-to 100 kHz have been reported recently [17]. Another aspect that is expected to improve in future is fast switching of wavelengths for PA spectroscopy. Novel techniques like delayed laser pulsing (per wavelength) are recently reported for avoiding movement artefacts during measurement using handheld probes [56]. Laser diode technology is also improving for providing pulsed light at higher rates and comparable energy [36]. However, repetition rate (thereby energy) is limited by the MPE. The frame rate of the system also depends upon how the system acquires and process (preprocess and reconstruct) the data for the final image. Developments in GPU (Graphical processing unit) and FPGA (Field Programmable Gate Array) technology are proving to be helpful in improving this, as parallel acquisition and processing is possible using these high-speed techniques. Compact, fast, and energy-efficient light sources together with sensitive and wide-band US signal detection, and high speed data acquisition and processing are the key factors for the translation of real-time PA/US imaging from research laboratories to clinics as a potential medical diagnostic technique.

Based on exciting early clinical investigation results, it is clear that PA/US imaging offers great promise in a wide range of clinical applications. The dual

modality can provide powerful molecular and functional imaging capabilities in the future. Future applications in the clinic may be in imaging for multiple indications like cardiovascular and peripheral vascular disease, disorders related to lymphatic system, breast lesions, arthritis and inflammation. It is foreseen that a real-time and handheld multi-wavelength dual modality PA/US system will make an impact on clinical patient care in the future.

Acknowledgments M. K. A. S. and W. S. are funded by the European Community's Seventh Framework Programme (FP7/2007-2013) under grant agreement no 318067. S. M. is funded by the Netherlands Organization for health research and development (ZonMw) under the program New Medical Devices for Affordable Health.

References

1. M.I. Mishchenko, L.D. Travis, A.A. Lacis, *Scattering, Absorption, and Emission of Light by Small Particles* (Cambridge University Press, Cambridge, 2002)
2. R. Weissleder, M.J. Pittet, Imaging in the era of molecular oncology. *Nature* **452**, 580–589 (2008)
3. R. Nachabe, B.H. Hendriks, M. Van Der Voort, A.E. Desjardins, H.J. Sterenberg, Estimation of biological chromophores using diffuse optical spectroscopy: Benefit of extending the uv-vis wavelength range to include 1000 to 1600 nm. *Biomed. Opt. Express* **1**, 1432–1442 (2010)
4. V. Baeriswyl, G. Christofori, The angiogenic switch in carcinogenesis. *Semin. Cancer Biol.* **19**, 329–337 (2009)
5. P. Carmeliet, R.K. Jain, Angiogenesis in cancer and other diseases. *Nature* **407**, 249–257 (2000)
6. N. Weidner, J.P. Semple, W.R. Welch, J. Folkman, Tumor angiogenesis and metastasis—correlation in invasive breast carcinoma. *N. Engl. J. Med.* **324**, 1–8 (1991)
7. P. Beard, Biomedical photoacoustic imaging. *Interface Focus* **1**, 602–631 (2011)
8. L.V. Wang, Tutorial on photoacoustic microscopy and computed tomography. *IEEE J. Sel. Top. Quantum Electron.* **14**, 171–179 (2008)
9. S. Ricci, L. Moro, R.A. Incalzi, Ultrasound imaging of the sural nerve: ultrasound anatomy and rationale for investigation. *Eur. J. Vasc. Endovasc. Surg.* **39**, 636–641 (2010)
10. J. Shalhoub, D.R.J. Owen, T. Gauthier, C. Monaco, E.L.S. Leen, A.H. Davies, The use of contrast enhanced ultrasound in carotid arterial disease. *Eur. J. Vasc. Endovasc. Surg.* **39**, 381–387 (2010)
11. T. Szabo, *Diagnostic Ultrasound Imaging: Inside Out* (Elsevier Academic, New York, NY, 2004)
12. M. Tanter, M. Fink, Ultrafast imaging in biomedical ultrasound. *IEEE Trans. Ultrason. Ferroelectr. Freq. Control* **61**, 102–119 (2014)
13. W. Xia, D. Piras, W. Steenbergen, T.G. van Leeuwen, S. Manohar, Photoacoustic imaging of the breast using the twente photoacoustic mammoscope: present status and future perspectives. *IEEE J. Sel. Top. Quantum Electron.* **16**, 730–739 (2010)
14. J.J. Xia, C.W. Wei, T.M. Nguyen, B. Arnal, I. Pelivanov, M. O'Donnell, Clinically translatable integrated ultrasound and photoacoustic imaging system. *Proc. SPIE* **8943**, 894310 (2014)
15. Y. Sun, H. Jiang, B.E. O'Neill, Photoacoustic imaging: an emerging optical modality in diagnostic and theranostic medicine. *J. Biosens. Bioelectron.* **2**, 108 (2011)
16. F.A. Duck, *Physical Properties of Tissue: A Comprehensive Reference Book* (Academic Press, London, 1990)

17. S. Manohar, S.E. Vaartjes, J.C. van Hespén, J.M. Klaase, F.M. van den Engh, W. Steenbergen, T.G. van Leeuwen, Initial results of in vivo non-invasive cancer imaging in the human breast using near-infrared photoacoustics. *Opt. Express* **15**, 12277–12285 (2007)
18. A.G. Bell, On the production and reproduction of sound by light. *Am. J. Sci.* **20**, 305–324 (1880)
19. R.A. Kruger, C. Appeldoorn, Photoacoustic ultrasound (PAUS)—reconstruction tomography. *Med. Phys.* **22**, 1605–1609 (1995)
20. A.A. Oraevsky, V.A. Andreev, A.A. Karabutov, R.D. Fleming, Z. Gatalica, H. Singh, R. O. Esenaliev, Laser optoacoustic imaging of breast: detection of cancer angiogenesis. *Proc. SPIE* **3597**, 352–363 (1999)
21. P. Beard, Photoacoustic imaging of blood vessel equivalent phantoms. *Proc. SPIE* **4618**, 55 (2002)
22. B.T. Cox, P.C. Beard, Fast calculation of pulsed photoacoustic fields in fluids using k-space methods. *J. Acoust. Soc. Am.* **117**, 3616–3627 (2005)
23. B.T. Cox, J.G. Laufer, P.C. Beard, The challenges for quantitative photoacoustic imaging. *Proc. SPIE* **7177**, 717713 (2009)
24. P. Kuchment, L. Kunyansky, A survey in mathematics for industry Mathematics of thermoacoustic tomography. *Eur. J. Appl. Math.* **19**, 191–224 (2008)
25. B.E. Treeby, B.T. Cox, k-Wave: MATLAB toolbox for the simulation and reconstruction of photoacoustic wave fields. *J. Biomed. Opt.* **15**, 021314 (2010)
26. C. Kim, T.N. Erpelding, L. Jankovic, M.D. Pashley, L.H.V. Wang, Deeply penetrating in vivo photoacoustic imaging using a clinical ultrasound array system. *Biomed. Opt. Express* **1**, 278–284 (2010)
27. J.J. Niederhauser, M. Jaeger, R. Lemor, P. Weber, M. Frenz, Combined ultrasound and optoacoustic system for real-time high-contrast vascular imaging in vivo. *IEEE Trans. Med. Imaging* **24**, 436–440 (2005)
28. C. Kim, T.N. Erpelding, L. Jankovic, L.V. Wang, Performance benchmarks of an array-based hand-held photoacoustic probe adapted from a clinical ultrasound system for non-invasive sentinel lymph node imaging. *Philos. Trans. R. Soc. Publishing Ser. A: Math. Phys. Eng. Sci.* **369**, 4644–4650 (2011)
29. R.J. Zemp, L.A. Song, R. Bitton, K.K. Shung, L.H.V. Wang, Realtime photoacoustic microscopy in vivo with a 30-MHz ultrasound array transducer. *Opt. Express* **16**, 7915–7928 (2008)
30. R.G.M. Kolkman, P.J. Brands, W. Steenbergen, T.G. van Leeuwen, Real-time photoacoustic & ultrasound imaging of human vasculature. *Proc. SPIE* **7177**, 717704 (2009)
31. S. Park, J. Shah, S.R. Aglyamov, A.B. Karpiouk, S. Mallidi, A. Gopal, H. Moon, X.J. Zhang, W.G. Scott, S.Y. Emelianov, Integrated system for ultrasonic, photoacoustic and elasticity imaging. *Proc. SPIE* **6147**, 61470H (2006)
32. J. Jose, R.G. Willemink, S. Resink, D. Piras, J.C. van Hespén, C.H. Slump, W. Steenbergen, T.G. van Leeuwen, S. Manohar, Passive element enriched photoacoustic computed tomography (PER PACT) for simultaneous imaging of acoustic propagation properties and light absorption. *Opt. Express* **19**, 2093–2104 (2011)
33. X.D. Wang, J.B. Fowlkes, J.M. Cannata, C.H. Hu, P.L. Carson, Photoacoustic imaging with a commercial ultrasound system and a custom probe. *Ultrasound Med. Biol.* **37**, 484–492 (2011)
34. K.P. Kostli, D. Frauchiger, J.J. Niederhauser, G. Paltauf, H.P. Weber, M. Frenz, Optoacoustic imaging using a three-dimensional reconstruction algorithm. *IEEE J. Sel. Top. Quantum Electron.* **7**, 918–923 (2001)
35. R.G.M. Kolkman, P.J. Brands, W. Steenbergen, T.G. van Leeuwen, Real-time in vivo photoacoustic and ultrasound imaging. *J. Biomed. Opt.* **13**, 050510 (2008)
36. K. Daoudi, P.J. van den Berg, O. Rabot, A. Kohl, S. Tisserand, P. Brands, W. Steenbergen, Handheld probe integrating laser diode and ultrasound transducer array for ultrasound/photoacoustic dual modality imaging. *Opt. Express* **22**, 26365–26374 (2014)
37. C. Haisch, K. Eilert-Zell, M.M. Vogel, P. Menzenbach, R. Niessner, Combined optoacoustic/ultrasound system for tomographic absorption measurements: possibilities and limitations. *Anal. Bioanal. Chem.* **397**, 1503–1510 (2010)

38. M.P. Fronheiser, S.A. Ermilov, H.P. Brecht, A. Conjusteau, R. Su, K. Mehta, A.A. Oraevsky, Real-time optoacoustic monitoring and three-dimensional mapping of a human arm vasculature. *J. Biomed. Opt.* **15**, 021305 (2010)
39. L.G. Montilla, R. Olafsson, D.R. Bauer, R.S. Witte, Real-time photoacoustic and ultrasound imaging: a simple solution for clinical ultrasound systems with linear arrays. *Phys. Med. Biol.* **58**, N1–N12 (2013)
40. A. Buehler, M. Kacprowicz, A. Taruttis, V. Ntziachristos, Real-time handheld multispectral optoacoustic imaging. *Opt. Lett.* **38**, 1404–1406 (2013)
41. A. Dima, V. Ntziachristos, Non-invasive carotid imaging using optoacoustic tomography. *Opt. Express* **20**, 25044–25057 (2012)
42. X.L. Dean-Ben, D. Razansky, Functional optoacoustic human angiography with handheld video rate three dimensional scanner. *Photoacoustics* **1**, 68–73 (2013)
43. X.L. Dean-Ben, D. Razansky, Adding fifth dimension to optoacoustic imaging: volumetric time-resolved spectrally enriched tomography. *Nat. Light: Sci. Appl.* **3**, e137 (2014)
44. A. Needles, A. Heinmiller, J. Sun, C. Theodoropoulos, D. Bates, D. Hirson, M. Yin, F.S. Foster, Development and initial application of a fully integrated photoacoustic micro-ultrasound system. *IEEE Trans. Ultrason. Ferroelectr. Freq. Control* **60**, 888–897 (2013)
45. G.C. Langhout, D.J. Grootendorst, O.E. Nieweg, M.W. Wouters, J.A. van der Hage, J. Jose, H. van Boven, W. Steenbergen, S. Manohar, T.J. Ruers, Detection of melanoma metastases in resected human lymph nodes by noninvasive multispectral photoacoustic imaging. *Int. J. Biomed. Imaging* **2014**, 163652 (2014)
46. J. Yuan, G. Xu, Y. Yu, Y. Zhou, P.L. Carson, X.D. Wang, X.J. Liu, Real-time photoacoustic and ultrasound dual-modality imaging system facilitated with graphics processing unit and code parallel optimization. *J. Biomed. Opt.* **18**, 086001 (2013)
47. G. Xu, J.R. Rajian, G. Girish, M.J. Kaplan, J.B. Fowlkes, P.L. Carson, X.D. Wang, Photoacoustic and ultrasound dual-modality imaging of human peripheral joints. *J. Biomed. Opt.* **18**, 010502 (2013)
48. Y. Cho, C.C. Chang, M. Jeon, C. Kim, L.H.V. Wang, J. Zou, A handheld optical fiber parallel acoustic delay line (PADL) probe for photoacoustic tomography. *Proc. SPIE* **8943**, 89432W (2014)
49. Y. Cho, C.C. Chang, J. Yu, M. Jeon, C. Kim, L.V. Wang, J. Zou, Handheld photoacoustic tomography probe built using optical-fiber parallel acoustic delay lines. *J. Biomed. Opt.* **19**, 086007 (2014)
50. J. Shah, S. Park, S. Aglyamov, T. Larson, L. Ma, K. Sokolov, K. Johnston, T. Milner, S.Y. Emelianov, Photoacoustic imaging and temperature measurement for photothermal cancer therapy. *J. Biomed. Opt.* **13**, 034024 (2008)
51. H.X. Ke, S. Tai, L.H.V. Wang, Photoacoustic thermography of tissue. *J. Biomed. Opt.* **19**, 026003 (2014)
52. A.A. Karabutov, E.V. Savateeva, N.B. Podymova, A.A. Oraevsky, Backward mode detection of laser-induced wide-band ultrasonic transients with optoacoustic transducer. *J. Appl. Phys.* **87**, 2003–2014 (2000)
53. W. Xia, D. Piras, J.C. van Hespren, S. van Veldhoven, C. Prins, T.G. van Leeuwen, W. Steenbergen, S. Manohar, An optimized ultrasound detector for photoacoustic breast tomography. *Med. Phys.* **40**, 032901 (2013)
54. S. Vaithilingam, T.J. Ma, Y. Furukawa, I.O. Wygant, X.F. Zhuang, A. De la Zerda, O. Oralkan, A. Kamaya, S.S. Gambhir, R.B. Jeffrey, B.T. Khuri-Yakub, Three-Dimensional Photoacoustic Imaging Using a Two-Dimensional CMUT Array. *IEEE Trans. Ultrason. Ferroelectr. Freq. Control* **56**, 2411–2419 (2009)
55. R. Bouchard, O. Sahin, S. Emelianov, Ultrasound-guided photoacoustic imaging: current state and future development. *IEEE Trans. Ultrason. Ferroelectr. Freq. Control* **61**, 450–466 (2014)
56. X.L. Dean-Ben, E. Bay, D. Razansky, Functional optoacoustic imaging of moving objects using microsecond-delay acquisition of multispectral three-dimensional tomographic data. *Nat. Sci. Rep.* **4**, 5878 (2014)